Chiral uncertainties in *ab initio* elastic nucleon-nucleus scattering

Robert B. Baker[1], Matthew Burrows[2], Charlotte Elster[1]*,
Kristina D. Launey[2], Pieter Maris[3], Gabriela Popa[1] and
Stephen P. Weppner[4]

[1]Department of Physics and Astronomy, Ohio University, Athens, OH, United States, [2]Department of Physics
and Astronomy, Louisiana State University, Baton Rouge, LA, United States, [3]Department of Physics and
Astronomy, Iowa State University, Ames, IA, United States, [4]Natural Sciences, Eckerd College, St. Petersburg,
FL, United States

The effective interaction between a nucleon and a nucleus is one of the most important ingredients for reaction theories. Theoretical formulations were introduced early by Feshbach and Watson, and efforts of deriving and computing those 'optical potentials' in a microscopic fashion have a long tradition. However, only recently the leading order term in the Watson multiple scattering approach could be calculated fully *ab initio*, meaning that the same nucleon-nucleon (NN) interaction enters both the structure as well as the reaction pieces on equal footing. This allows the uncertainties from the underlying chiral effective NN interaction to be systematically explored in nucleon-nucleus elastic scattering observables. In this contribution the main ingredients for arriving at the *ab initio* leading order of the effective nucleon-nucleus interaction in the Watson approach will be reviewed. Concentrating on one specific chiral NN interaction from the LENPIC collaboration and light nuclei with a 0^+ ground state, the leading order nucleon-nucleus interaction is calculated using up to the third chiral order (N2LO) in the nucleon-nucleon potential, and elastic scattering observables are extracted. Then pointwise as well as correlated uncertainty quantification is used for the estimation of the chiral truncation error. Elastic scattering observables for ^{4}He, ^{12}C, and ^{16}O for between 65 and 200 MeV projectile energy will be analyzed.

1 Introduction

Simplifying the many-body problem posed by scattering of a proton or neutron from a nucleus to a two-body problem with an effective (optical) potential was introduced already by Bethe [1] in the 1930s, and its justification summarized by Feshbach [2]. Since then differential cross sections as well as spin observables for elastic scattering played an important role in either determining the parameters in phenomenological optical models for proton or neutron scattering from nuclei or in testing validity and accuracy of microscopic models thereof. The theoretical approach to elastic scattering from a nuclear target presented in this article is based on the ansatz of a multiple scattering expansion that was pioneered by Watson [3, 4], made familiar by Kerman, McManus, and Thaler (KMT) [5]. and refined further as spectator expansion [6–8]. Specifically, elastic scattering from stable nuclei has led in the 1990s to a large body of work on microscopic optical potentials in which the nucleon-nucleon interaction and the density of the nucleus were taken as input to rigorous calculations of first-order potentials, in either a Kerman-McManus-Thaler (KMT) or a Watson expansion of the multiple scattering series (see e.g. [9–14]). Here the primary goal was a deeper understanding of the reaction

mechanism. However, a main disadvantage of that work was the lack of sophisticated nuclear structure input compared to what is available today.

Recent developments of the nucleon-nucleon (NN) and three-nucleon (3N) interactions, derived from chiral effective field theory, have yielded major progress [15–22]. These, together with the utilization of massively parallel computing resources (e.g., see [23–27]), have placed *ab initio* large-scale simulations at the frontier of nuclear structure and reaction explorations. Among other successful many-body theories, the *ab initio* no-core shell-model (NCSM) approach (see, e.g. [28–31]), has over the last decade taken center stage in the development of microscopic tools for studying the structure of atomic nuclei. The NCSM concept combined with a symmetry-adapted (SA) basis in the *ab initio* SA-NCSM [32] has further expanded the reach to the structure of intermediate-mass nuclei [33].

Following the developments in nuclear structure theory, it is very natural to again consider rigorous calculations of effective folding nucleon-nucleus (NA) potentials, since now the nuclear densities required as input for the folding with the NN scattering amplitudes can be based on the same chiral NN interaction. This development also allows to investigate effects of truncation uncertainties in the chiral expansion on NA scattering observables in a similar fashion as already successfully performed in NN scattering (see e.g. [34–36]), nucleon-deuteron scattering [37], or structure observables for light nuclei [31, 38].

The theoretical and computational developments leading to *ab initio* NA effective interactions (in leading order in the spectator expansion) are described in a serious of publications by the authors [39–43] and others (see e. g. [44–47]). Thus the aim of this review is to shed light on truncation uncertainties in the chiral expansion, and within that context give a perspective on intricacies of the spectator expansion as well as the explicit content of its leading order term, which can now be calculated *ab initio*.

Deriving *ab initio* optical potentials within a multiple scattering approach focuses on projectile energies at energies about 80 MeV or higher, since the expectation is that at those energies the leading order term may already capture the most important physics. Another recent *ab initio* approach starts from a formulation introduced by Feshbach [48] and constructs optical potentials and elastic scattering observables within a Green's function approach [49, 50]. For elastic scattering from medium-mass nuclei the coupled-cluster method [51] and the SA-NCSM [52] approach have been successfully implemented. These approaches are by design better suited for calculating scattering observables at energies below about 20–30 MeV due to restrictions on the size of the model spaces which increase with increasing projectile energy. In Ref. [53] an extensive overview of the status of the field of optical potentials and their need in the rare-isotope era is given and the current status of *ab initio* approaches is discussed. We want to encourage the reader to refer to this work, for more details.

2 Watson optical potential within the spectator expansion

The standard starting point for describing elastic scattering of a single projectile from a target of A particles within a multiple scattering approach is the separation of the Lippmann-Schwinger (LS) equation for the transition operator T,

$$T = V + VG_0(E)T \tag{1}$$

into two parts, namely an integral equation for T,

$$T = U + UG_0(E)PT, \tag{2}$$

where U is the effective potential operator defined by a second integral equation,

$$U = V + VG_0(E)QU. \tag{3}$$

Here p is a projection onto the ground state of the target, $P = \frac{|\Phi_0\rangle\langle\Phi_0|}{\langle\Phi_0|\Phi_0\rangle}$, with $P + Q = 1$ and $[G_0(E), P] = 1$. The free propagator for the projectile and target system is given by $G_0(E) = (E - h_0 - H_A + i\epsilon)^{-1}$ where h_0 is the kinetic energy of the projectile and H_A is the Hamiltonian of the target nucleus. The general solutions of the nuclear bound state problem $H_A|\Phi\rangle$ include the ground state, excited states and continuum states. For the scattering problem given by the transition amplitude T the reference energy separating bound and continuum states is chosen such that the ground state energy is set to zero. Thus energies referring to the target Hamiltonian in G_0 are excitation energies of the target. With these definitions the transition operator for elastic scattering may be redefined as $T_{\text{el}} = PTP$, in which case Eq. 2 can be written as

$$T_{\text{el}} = PUP + PUPG_0(E)T_{\text{el}}. \tag{4}$$

2.1 Spectator expansion of the operator U

The transition operator for elastic scattering is given by a straightforward one-body integral equation, which of course requires the knowledge of PUP, which is a many-body operator. For a brief review we follow the spectator expansion of PUP as introduced in Ref. [54] in contrast to Ref. [6] where the expansion of T is considered. Following those references, we assume the presence of two-body forces only for the present discussion. The extension to many-body forces is not precluded by the formulation. With this assumption the operator U can be expanded as

$$U = \sum_{i=1}^{A} U_i, \tag{5}$$

where U_i is given by

$$U_i = v_{0i} + v_{0i}G_0(E)Q\sum_{j=1}^{A} U_j, \tag{6}$$

provided that $V = \sum_{i=1}^{A} v_{0i}$, where the two-body potential v_{0i} acts between the projectile and the ith target nucleon. Through the introduction of an operator τ_i which satisfies

$$\tau_i = v_{0i} + v_{0i}G_0(E)Q\tau_i, \tag{7}$$

Eq. 6 can be rearranged as

$$U_i = \tau_i + \tau_i G_0(E)Q\sum_{j\neq i} U_j. \tag{8}$$

This rearrangement process can be continued for all A target particles, so that the operator for the optical potential can be expanded in a series of A terms of the form
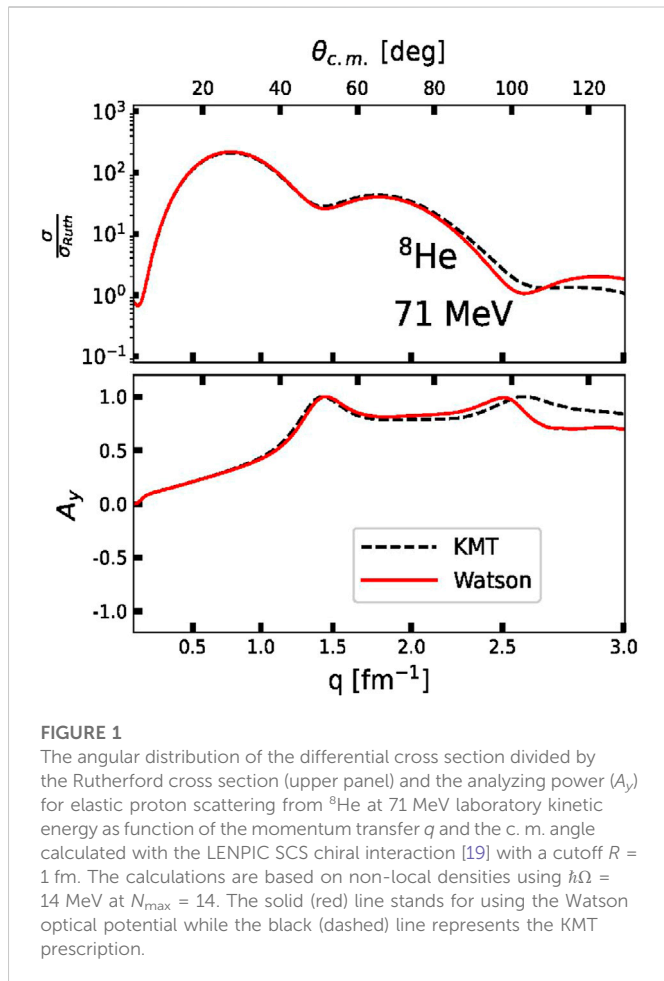
FIGURE 1
The angular distribution of the differential cross section divided by the Rutherford cross section (upper panel) and the analyzing power (A_y) for elastic proton scattering from ^{8}He at 71 MeV laboratory kinetic energy as function of the momentum transfer q and the c. m. angle calculated with the LENPIC SCS chiral interaction [19] with a cutoff $R = 1$ fm. The calculations are based on non-local densities using $\hbar\Omega = 14$ MeV at $N_{max} = 14$. The solid (red) line stands for using the Watson optical potential while the black (dashed) line represents the KMT prescription.

$$U = \sum_{i=1}^{A} \tau_i + \sum_{i,j\neq i}^{A} \tau_{ij} + \sum_{i,j\neq i,k\neq i,j}^{A} \tau_{ijk} + \cdots. \qquad (9)$$

This is the Spectator Expansion for U, where each term is treated in turn. The separation of the interactions according to the number of interacting nucleons has a certain latitude, due to the many-body nature of $G_0(E)$, which needs to be considered separately. In the following we will concentrate on the leading-order term, which is still a many-body operator due the presence of $G_0(E)$. The next-to-leading order term in this spectator expansion for U has been formally derived and connected to standard three-body equations in Ref. [54].

2.2 Propagator expansion in the leading-order term of U

When using the leading-order term of the spectator expansion as given in Eq. 7, for elastic scattering only $P\tau_i P$, or equivalently $\langle\Phi_0|\tau_i|\Phi_0\rangle$ needs be considered. With this in mind, Eq. 7 can be re-expressed as

$$\tau_i = \nu_{0i} + \nu_{0i}G_0(E)\tau_i - \nu_{0i}G_0(E)P\tau_i = \hat{\tau}_i - \hat{\tau}_iG_0(E)P\tau_i, \qquad (10)$$

or

$$\langle\Phi_0|\tau_i|\Phi_0\rangle = \langle\Phi_0|\hat{\tau}_i|\Phi_0\rangle - \langle\Phi_0|\hat{\tau}_i|\Phi_0\rangle\frac{1}{(E-E_A)-h_0+i\varepsilon}\langle\Phi_0|\tau_i|\Phi_0\rangle, \qquad (11)$$

where $\hat{\tau}_i$ is defined as the solution of

$$\hat{\tau}_i = \nu_{0i} + \nu_{0i}G_0(E)\hat{\tau}_i. \qquad (12)$$

The combination of Eqs 10, 2 corresponds to the leading-order Watson optical potential [3, 4]. In *ab initio* structure calculations the one-body densities or ground state wave functions for protons and neutrons are calculated separately, so that Eq. 11 allows to combine e.g. for proton scattering of a nucleus the proton-neutron interaction ($\hat{\tau}_{i=pn}$) with the neutron one-body density and the proton-proton interaction with the proton one-body density. The sum over i then adds both to obtain the driving term $\langle\Phi_0|\hat{\tau}_i|\Phi_0\rangle$ the integral equation, Eq. 11.

If the projectile-target-nucleon interaction is assumed to be the same for all target nucleons and if iso-spin effects are neglected then the KMT approximation ($\frac{A-1}{A}\langle\Phi_0|\hat{\tau}_i|\Phi_0\rangle$) can be derived from the leading-order Watson potential [5]. When working with momentum space integral equations, the numerical implementation of Eq. 11 is straightforward [40, 41, 45, 55]. Working in coordinate space with differential equations does not allow an equally straightforward implementation, and thus the KMT prescription is the most favorable alternative. A comparison between leading-order Watson potential and the KMT prescription is shown in Figure 1 for elastic proton scattering from ^{8}He at 71 MeV laboratory kinetic energy. Despite the relatively large difference between the proton and neutron densities for this nucleus the KMT prescription agrees with the exact Watson description very well up to momentum transfers of about 2 fm^{-1}.

Since Eq. 11 is a one-body integral equation, the principal problem is to find a solution of Eq. 12, which due to many-body character of $G_0(E)$ is still a many-body integral equation, and in fact no more easily solved than the starting point of Eq. 1.

For most practical calculations the so-called closure approximation to $G_0(E)$ is implemented [56] turning Eq. 12 into a one-body integral equation. This approximation replaces H_A by a constant that is interpreted as an average excitation energy, and is justified when the projectile energy is large compared to typical excitation energies of the nucleus. The closure approximation is very successfully applied for elastic scattering around 80 MeV and higher.

Going beyond the closure approximation in the spirit of the spectator expansion we want to single out one target nucleon i and write $G_0(E)$ as

$$G_0(E) = (E - h_0 - H_A + i\varepsilon)^{-1}$$
$$= \left(E - h_0 - h_i - \sum_{j\neq i}\nu_{ij} - H^i + i\varepsilon\right)^{-1}, \qquad (13)$$

where the target Hamiltonian is expanded as $H_A = h_i + \sum_{j\neq i}\nu_{ij} + H^i$ with ν_{ij} being the interaction between target nucleons i and j, and H^i being an $(A-1)$-body operator containing all higher order effects. Realizing that $\sum_{j\neq i}\nu_{ij} \equiv W_i$ and thus $H^i = H_A - h_i - W_i$ does not have an explicit dependence on the ith particle, then H^i may be replaced by an average energy E^i which is akin to the effective binding energy between the ith nucleon and the $A-1$ spectator. This is not an approximation since $G_0(E)$ may be regarded as

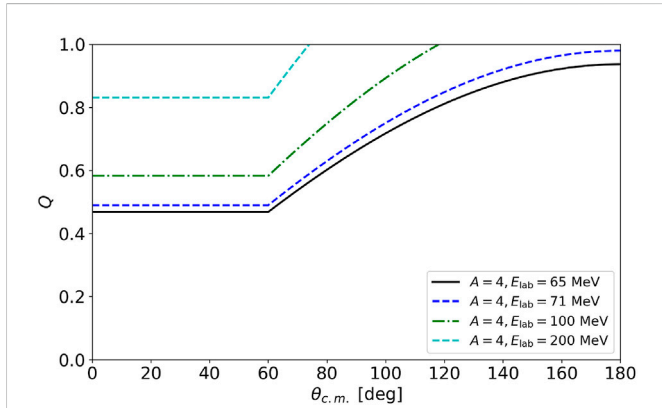$$G_0(E) = \left[(E - E^i) - h_0 - h_i - W_i - (H^i - E^i) + i\varepsilon\right]^{-1} \qquad (14)$$

FIGURE 2
The expansion parameter Q, defined by Eq. 30 where $\Lambda_b =$ x600 MeV, as a function of the center-of-mass angle $\theta_{c.m.}$ for a range of lab projectile energies E_{lab}. In this case of nucleon-nucleus (NA) elastic scattering, the transition between when the expansion parameter is dominated by the center-of-mass momentum and the momentum transfer can easily be identified.

and $(H^i − E^i)$ should be set aside to be treated in the next order of the expansion of the propagator $G_0(E)$. In this order of the expansion $G_0(E)$ becomes

$$G_i(E) = \left[(E − E^i) − h_0 − h_i − W_i + i\varepsilon\right]^{-1}, \tag{15}$$

and Eq. 12 reads

$$\hat{\tau}_i = v_{0i} + v_{0i} G_i(E)\hat{\tau}_i. \tag{16}$$

In order to connect the above expression with the free NN amplitude

$$t_{0i} = v_{0i} + v_{0i} g_i t_{0i} \tag{17}$$

with

$$g_i = \left[(E − E^i) − h_0 − h_i + i\varepsilon\right]^{-1}. \tag{18}$$

algebraic relations between the resolvents lead to

$$\hat{\tau}_i = t_{0i} + t_{0i} G_i W_i g_i(E)\hat{\tau}_i. \tag{19}$$

Defining $G_i W_i = g_i \mathcal{T}_i$ with $\mathcal{T}_i = W_i + W_i g_i \mathcal{T}_i$ leads to

$$\hat{\tau}_i = t_{0i} + t_{0i} g_i \mathcal{T}_i g_i \hat{\tau}_i. \tag{20}$$

The three-body character of the above expression becomes more evident if one defines it as a set of coupled equations as

$$\begin{aligned} \hat{\tau}_i &= t_{0i} + t_{0i} g_i X_i \\ X_i &= \mathcal{T}_i g_i \hat{\tau}_i. \end{aligned} \tag{21}$$

Though the spectator expansion of the operator U in terms of active particles is defined in Eq. 9, we see that this expansion is performed in terms of quantities which contain many-body propagators. Each of the ingredients τ_i, τ_{ij}, etc. may themselves be expanded in a spectator expansion, i.e. expanding the many-body propagator also according to the number of active participants. The corrections to the propagator in the leading-order term of U contributions that arise from the Q space, whereas the terms arising from the propagator remain in the P space at first order level. Thus their contribution may be more relevant for elastic scattering.

In an explicit treatment of $G_i(E)$ it is necessary to consider the explicit form of $\sum_{j\neq i} v_{ij} = W_i$, which is *a priori* a two-body operator. In the framework of *ab initio* nuclear structure calculations this will involve two-body densities. In earlier work [54, 57, 58] the quantity W_i was treated as one-body operator, specifically a mean-field potential. This was a physically reasonable choice, though being outside the strict demands of the spectator expansion. However, those studies revealed that the next order in the propagator expansion has little effect on elastic scattering observables at energies larger than 100 MeV, while the description of differential cross section and spin-observables for elastic scattering from ^{40}Ca at 48 MeV showed considerable improvement with respect to experiment [57]. Obviously this type of calculation will need to be explored within an *ab initio* approach. In Ref. [57] the energy E^i of Eq. 18 was set to zero.

As illustrated in this section, deriving a multiple scattering expansion for elastic NA scattering means projecting on the ground state of the target in order to obtain a Lippman-Schwinger type equation for the transition amplitude and obtaining an operator U for the effective interaction, which is defined in the space $Q = 1 − P$. In this spirit, the spectator expansion contains therefore two pieces, namely the expansion of the operator U in terms of active particles in the scattering process as well as the expansion of target Hamiltonian H_A in the propagator $G_0(E)$ in a similar fashion. Thus it is very difficult to define a single expansion parameter which governs the convergence of the expansion.
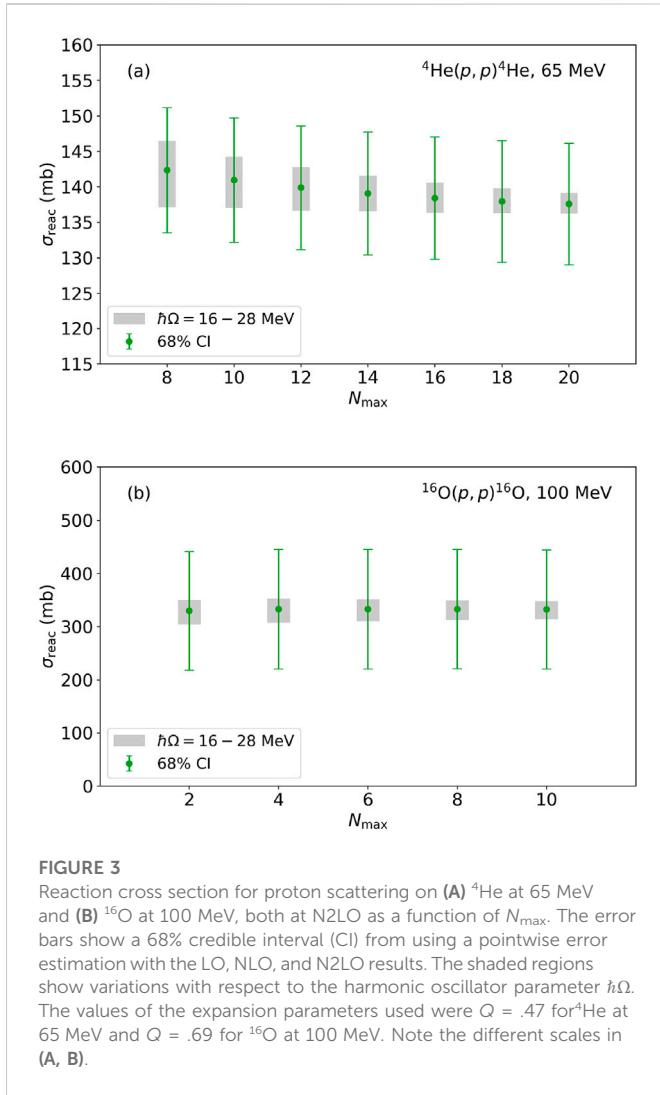
3 Leading order *ab initio* optical potential based on a chiral NN interaction

The leading order of the spectator expansion involves two active nucleons, the projectile and a target nucleon. Therefore, the leading order is driven by the NN amplitude $\bar{M}$, which in its most general form can be parameterized in terms of Wolfenstein amplitudes [59–61],

$$\begin{aligned} \bar{M}(\boldsymbol{q}, \mathcal{K}_{NN}, \epsilon) = &\, A(\boldsymbol{q}, \mathcal{K}_{NN}, \epsilon)\mathbf{1} \otimes \mathbf{1} \\ &+ iC(\boldsymbol{q}, \mathcal{K}_{NN}, \epsilon)\,(\boldsymbol{\sigma}^{(0)} \cdot \hat{\boldsymbol{n}}) \otimes \mathbf{1} \\ &+ iC(\boldsymbol{q}, \mathcal{K}_{NN}, \epsilon)\,\mathbf{1} \otimes (\boldsymbol{\sigma}^{(i)} \cdot \hat{\boldsymbol{n}}) \\ &+ M(\boldsymbol{q}, \mathcal{K}_{NN}, \epsilon)(\boldsymbol{\sigma}^{(0)} \cdot \hat{\boldsymbol{n}}) \otimes (\boldsymbol{\sigma}^{(i)} \cdot \hat{\boldsymbol{n}}) \\ &+ [G(\boldsymbol{q}, \mathcal{K}_{NN}, \epsilon) − H(\boldsymbol{q}, \mathcal{K}_{NN}, \epsilon)] \\ &\quad \times (\boldsymbol{\sigma}^{(0)} \cdot \hat{\boldsymbol{q}}) \otimes (\boldsymbol{\sigma}^{(i)} \cdot \hat{\boldsymbol{q}}) \\ &+ [G(\boldsymbol{q}, \mathcal{K}_{NN}, \epsilon) + H(\boldsymbol{q}, \mathcal{K}_{NN}, \epsilon)] \\ &\quad \times (\boldsymbol{\sigma}^{(0)} \cdot \hat{\mathcal{K}}) \otimes (\boldsymbol{\sigma}^{(i)} \cdot \hat{\mathcal{K}}) \\ &+ D(\boldsymbol{q}, \mathcal{K}_{NN}, \epsilon)[(\boldsymbol{\sigma}^{(0)} \cdot \hat{\boldsymbol{q}}) \otimes (\boldsymbol{\sigma}^{(i)} \cdot \hat{\mathcal{K}}) \\ &+ (\boldsymbol{\sigma}^{(0)} \cdot \hat{\mathcal{K}}) \otimes (\boldsymbol{\sigma}^{(i)} \cdot \hat{\boldsymbol{q}})], \end{aligned} \tag{22}$$

where $\boldsymbol{\sigma}^{(0)}$ describes the spin of the projectile, and $\boldsymbol{\sigma}^{(i)}$ the spin of the struck nucleon. The average momentum in the NN frame is defined as $\mathcal{K}_{NN} = \frac{1}{2}(\boldsymbol{k}'_{NN} + \boldsymbol{k}_{NN})$. The scalar functions A, C, M, G, H, and D are referred to as Wolfenstein amplitudes and only depend on the scattering momenta and energy. Each term in Eq. 22 has two components, namely a scalar function of two vector momenta and an energy and the coupling between the operators of the projectile and the struck nucleon. The linear independent unit vectors $\hat{\boldsymbol{q}}$, $\hat{\mathcal{K}}$, and $\hat{\boldsymbol{n}}$ are defined in terms of the momentum transfer and the average momentum as

$$\hat{\boldsymbol{q}} = \frac{\boldsymbol{q}}{|\boldsymbol{q}|} \quad , \quad \hat{\mathcal{K}} = \frac{\mathcal{K}}{|\mathcal{K}|} \quad , \quad \hat{\boldsymbol{n}} = \frac{\mathcal{K} \times \boldsymbol{q}}{|\mathcal{K} \times \boldsymbol{q}|}, \tag{23}$$

FIGURE 3
Reaction cross section for proton scattering on **(A)** ^{4}He at 65 MeV and **(B)** ^{16}O at 100 MeV, both at N2LO as a function of $N_{\max}$. The error bars show a 68% credible interval (CI) from using a pointwise error estimation with the LO, NLO, and N2LO results. The shaded regions show variations with respect to the harmonic oscillator parameter $\hbar\Omega$. The values of the expansion parameters used were $Q = .47$ for^{4}He at 65 MeV and $Q = .69$ for ^{16}O at 100 MeV. Note the different scales in **(A, B)**.

and span the momentum vector space. With the exception of the momentum transfer $\boldsymbol{q}$, which is invariant under frame transformation, the vectors in Eq. 23 need to be considered in their respective frame in explicit calculations [41, 62]. For the struck target nucleon the expectation values of the operator **one** and the scalar products of $\boldsymbol{\sigma}^{(i)}$ with the linear independent unit vectors of Eq. 23 need to be evaluated with the ground state wave functions of the respective nucleus when calculating the leading-order NA effective interaction. Evaluating the expectation value of the operator **one** in the ground state of the nucleus results in the scalar non-local, translationally invariant one-body density that has traditionally been used as input to microscopic or *ab initio* calculations of leading order effective interactions [11, 12, 40, 44]. The other operators from Eq. 23, namely $(\boldsymbol{\sigma}^{(i)} \cdot \hat{\boldsymbol{n}})$, $(\boldsymbol{\sigma}^{(i)} \cdot \hat{\boldsymbol{q}})$, and $(\boldsymbol{\sigma}^{(i)} \cdot \hat{\mathcal{K}})$ need to also be evaluated for a leading-order *ab initio* NA effective interaction, in which the NN interaction is treated on equal footing in the reaction and structure calculation.

Thus, the general expression for a non-local density needs to include the spin operator $\boldsymbol{\sigma}^{(i)}$ explicitly,

$$\rho_{q_s}^{K_s}(\boldsymbol{p},\boldsymbol{p}') = \left\langle \Phi_0' \left| \sum_{i=1}^{A} \delta^3(\boldsymbol{p}_i - \boldsymbol{p})\delta^3(\boldsymbol{p}_i' - \boldsymbol{p}')\sigma_{q_s}^{(i)K_s} \right| \Phi_0 \right\rangle, \quad (24)$$

where $\sigma_{q_s}^{(i)K_s}$ is the spherical representation of the spin operator and the wavefunction $\Phi_0(\boldsymbol{p}_1, \ldots, \boldsymbol{p}_A) = \langle \boldsymbol{p}_1, \ldots, \boldsymbol{p}_A | \Phi_0 \rangle$ is defined in momentum space. Evaluating this expression for $K_s = 0$ gives the non-local one-body scalar density and $K_s = 1$ becomes a non-local one-body spin density.

The Wolfenstein parameterization of Eq. 22 requires the evaluation of scalar products of the one-body spin density with unit momentum vectors. Since those only depend on the momenta $\boldsymbol{p}$ and $\boldsymbol{p}'$, those can be calculated as $\rho^{K_s}(\boldsymbol{p},\boldsymbol{p}') \cdot \hat{\boldsymbol{n}}$, $\rho^{K_s}(\boldsymbol{p},\boldsymbol{p}') \cdot \hat{\boldsymbol{q}}$, and $\rho^{K_s}(\boldsymbol{p},\boldsymbol{p}') \cdot \hat{\mathcal{K}}$. For the explicit calculation of $\rho^{K_s}(\boldsymbol{p},\boldsymbol{p}') \cdot \hat{\boldsymbol{n}}$, we refer the reader to [41, 62]. The scalar products $(\boldsymbol{\sigma}^{(i)} \cdot \hat{\boldsymbol{q}})$ and $(\boldsymbol{\sigma}^{(i)} \cdot \hat{\mathcal{K}})$ represent scalar products of a pseudo-vector and a vector, a construct that is not invariant under parity transformations, and thus vanish when sandwiched between ground state wave functions, which is explicitly shown in [62]. Thus the tensor contributions of the NN force only enter the leading order effective NA interaction through the Wolfenstein amplitude M as long as elastic scattering is considered. When e.g. transition amplitudes between states of different parity would be considered, the other tensor amplitudes will contribute.

Currently contributions to elastic scattering observables due to the spin-projected one-body densities have only been calculated for light nuclei with 0^+ ground states, and it was found that this contribution is very small for nuclei with equal proton and neutron numbers [41, 42]. This is likely different for nuclei with ground states of non-zero spin, which was explored for ^{10}B polarization transfer observables in Refs. [63, 64], where the authors assume a nuclear structure which consists of a core and valence nucleons. The work of Ref. [45] extends the standard leading order calculation to non-zero spin nuclei, however does not consider the inherent tensor contributions from the NN force in their formulation. This leaves the importance of a consistent treatment of the NN force on elastic scattering from non-zero spin nuclei still an open question.

The complete calculation of the leading-order effective interaction describing the scattering of a proton from a nucleus in a 0^+ ground state and which enters the integral Eq. 11 as driving term is given by

$$\begin{aligned}
\hat{U}_{\mathrm{p}}(\boldsymbol{q},\mathcal{K}_{NA},\epsilon) = & \sum_{\alpha=\mathrm{n,p}} \int d^3\mathcal{K}\eta(\boldsymbol{q},\mathcal{K},\mathcal{K}_{NA})A_{\mathrm{p}\alpha}\left(\boldsymbol{q},\frac{1}{2}\left(\frac{A+1}{A}\mathcal{K}_{NA}-\mathcal{K}\right);\epsilon\right)\rho_{\alpha}^{K_s=0}(\mathcal{P}',\mathcal{P}) \\
& + i\left(\boldsymbol{\sigma}^{(0)}\cdot\hat{\boldsymbol{n}}\right)\times\sum_{\alpha=\mathrm{n,p}} \int d^3\mathcal{K}\eta(\boldsymbol{q},\mathcal{K},\mathcal{K}_{NA})C_{\mathrm{p}\alpha}\left(\boldsymbol{q},\frac{1}{2}\left(\frac{A+1}{A}\mathcal{K}_{NA}-\mathcal{K}\right);\epsilon\right)\rho_{\alpha}^{K_s=0}(\mathcal{P}',\mathcal{P}) \\
& + i\sum_{\alpha=\mathrm{n,p}} \int d^3\mathcal{K}\eta(\boldsymbol{q},\mathcal{K},\mathcal{K}_{NA})C_{\mathrm{p}\alpha}\left(\boldsymbol{q},\frac{1}{2}\left(\frac{A+1}{A}\mathcal{K}_{NA}-\mathcal{K}\right);\epsilon\right)S_{n,\alpha}(\mathcal{P}',\mathcal{P})\cos\beta \\
& + i\left(\boldsymbol{\sigma}^{(0)}\cdot\hat{\boldsymbol{n}}\right)\sum_{\alpha=\mathrm{n,p}} \int d^3\mathcal{K}\eta(\boldsymbol{q},\mathcal{K},\mathcal{K}_{NA}) \\
& \times(-i)M_{\mathrm{p}\alpha}\left(\boldsymbol{q},\frac{1}{2}\left(\frac{A+1}{A}\mathcal{K}_{NA}-\mathcal{K}\right);\epsilon\right)S_{n,\alpha}(\mathcal{P}',\mathcal{P})\cos\beta.
\end{aligned} \quad (25)$$

The term $\eta(\boldsymbol{q},\mathcal{K},\mathcal{K}_{NA})$ is the Møller factor [65] describing the transformation from the NN frame to the NA frame. The functions $A_{\mathrm{p}\alpha}$, $C_{\mathrm{p}\alpha}$, and $M_{\mathrm{p}\alpha}$ represent the NN interaction through Wolfenstein amplitudes [59]. Since the incoming proton can interact with either a proton or a neutron in the nucleus, the index α indicates the neutron (n) and proton (p) contributions, which are calculated

separately and then summed up. With respect to the nucleus, the operator $i(\boldsymbol{\sigma}^{(0)} \cdot \hat{\boldsymbol{n}})$ represents the spin-orbit operator in momentum space with respect to the projectile. As such, Eq. 25 exhibits the expected form of an interaction between a spin-$\frac{1}{2}$ projectile and a target nucleus in a $J = 0$ state [66]. The momentum variables in the problem are given as

$$
\begin{aligned}
\boldsymbol{q} &= \boldsymbol{p}' - \boldsymbol{p} = \boldsymbol{k}' - \boldsymbol{k}, \\
\mathcal{K} &= \frac{1}{2}(\boldsymbol{p}' + \boldsymbol{p}), \\
\mathcal{K}_{NA} &= \frac{A}{A+1}\left[(\boldsymbol{k}' + \boldsymbol{k}) + \frac{1}{2}(\boldsymbol{p}' + \boldsymbol{p})\right], \\
\mathcal{P} &= \mathcal{K} + \frac{A-1}{A}\frac{\boldsymbol{q}}{2}, \\
\mathcal{P}' &= \mathcal{K} - \frac{A-1}{A}\frac{\boldsymbol{q}}{2}.
\end{aligned}
\tag{26}
$$

The two quantities representing the structure of the nucleus are the scalar one-body density $\rho_\alpha^{K_s=0}(\mathcal{P}', \mathcal{P})$ and the spin-projected momentum distribution $S_{n,\alpha}(\mathcal{P}', \mathcal{P}) = \rho^{K_s=1}(\mathcal{P}', \mathcal{P}) \cdot \hat{\boldsymbol{n}}$. Both distributions are non-local and translationally invariant. The reduced matrix elements entering the one-body densities are obtained within the NCSM (SA-NCSM) in the center-of-mass frame of the nucleus. In order to employ them in calculating the leading-order effective NA interaction, this center-of-mass variable must be removed. Within the framework of NCSM (SA-NCSM) the technique for obtaining non-local and translationally invariant one-body densities is well developed [40, 44, 67–70]. Lastly, the term $\cos\beta$ in Eq. 25 results from projecting $\hat{\boldsymbol{n}}$ from the NN frame to the NA frame. For further details, see Ref. [41].

4 Chiral truncation uncertainties in the leading order optical potential

With the emergence of nuclear forces based on chiral effective field theory (EFT), we are presented with an opportunity to study the nucleon-nucleus effective interaction as it develops order-by-order in a chiral EFT framework. Given the hierarchical nature of chiral EFT, we can combine these order-by-order results to reliably estimate truncation uncertainties associated with the higher chiral orders not included in the calculations. To this end, Refs. [35–37] first implemented uncertainty quantification for the cases of NN and Nd scattering by assuming a quantity $y(x)$ at a chiral order k can be written as

$$
y_k(x) = y_{\text{ref}}(x) \sum_{n=0}^{k} c_n(x) Q^n(x)
\tag{27}
$$

where $y_{\text{ref}}(x)$ is a reference value that sets the scale of the problem and also includes the dimensions of the quantity $y(x)$ of interest. By construction, the coefficients $c_n(x)$ are dimensionless and are expected to be of order unity. The remaining quantity $Q(x)$ is the expansion parameter associated with the chiral EFT. The expansion parameter is usually defined as

$$
Q = \frac{1}{\Lambda_b} \max(M_\pi, p)
\tag{28}
$$

where Λ_b is the breakdown scale of the EFT, M_π is the pion mass, and p is the relevant momentum for the problem. Various works [35–37] have identified the relevant momentum in different ways, but keeping with Ref. [43] we choose the relevant momentum as

TABLE 1 Ground state binding energies (top) and point-proton RMS radii (bottom) of ^{4}He, ^{12}C, and ^{16}O with LO, NLO, and N^{2}LO LENPIC SCS NN potentials. Both our estimated numerical uncertainties (first set of uncertainties) and chiral truncation uncertainty estimates (second set of uncertainties, not evaluated for LO) are given.

	^{4}He	^{12}C	^{16}O
	Binding energy (MeV)		
LO	45.45(.01)	137.(1.)	224.(2.)
NLO	28.53(.01)(3.5)	97.(3.)(9.)	156.(5.)(14.)
N^{2}LO	28.11(.01)(.9)	94.(4.)(3.)	149.(5.)(4.)
expt	28.30	92.16	127.62
	Point-proton radius (fm)		
LO	1.08(.02)	1.85(.17)	1.8(.2)
NLO	1.40(.02)(.08)	2.04(.16)(.09)	2.05(.16)(.10)
N^{2}LO	1.42(.02)(.02)	2.12(.15)(.03)	2.11(.15)(.03)
expt	1.46	2.32	2.58

the center-of-mass (c.m.) momentum in the nucleon-nucleus system

$$
p_{NA}^2 = \frac{E_{\text{lab}} A^2 m^2 (E_{\text{lab}} + 2m)}{m^2 (A+1)^2 + 2AmE_{\text{lab}}}
\tag{29}
$$

where E_{lab} is the kinetic energy of the projectile in the laboratory frame, A is the target nucleus's mass number, and m is the mass of the nucleon.
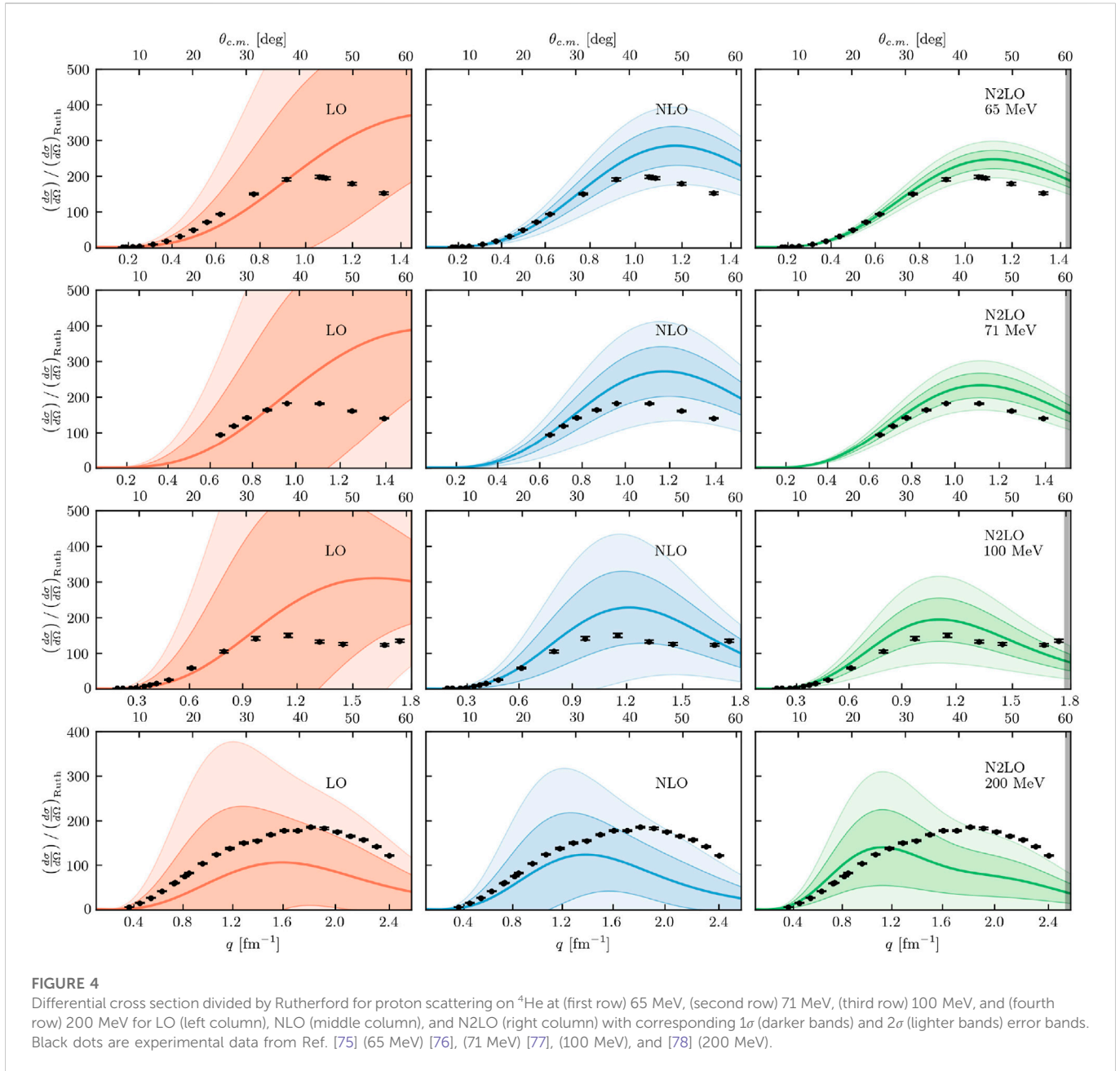
Previous scattering works [36, 43] have noted that various results indicate, when identifying the relevant momentum, the momentum transfer q should also be considered. That is, the expansion parameter would be more appropriately defined as

$$
Q = \frac{1}{\Lambda_b} \max(M_\pi, p_{NA}, q)
\tag{30}
$$

The momentum transfer in elastic scattering is defined as

$$
q = 2 p_{NA} \sin\left(\frac{\theta_{\text{c.m.}}}{2}\right)
\tag{31}
$$

where $\theta_{\text{c.m.}}$ is the scattering angle in the c. m. frame. Notably, including the momentum transfer in Eq. 30 makes the expansion parameter a function of $\theta_{\text{c.m.}}$, even though the other momentum scales in Eq. 30 are independent of the scattering angle. When considering observables such as the differential cross section or analyzing power that are functions of $\theta_{\text{c.m.}}$, this implies the expansion parameter will be larger at backward angles than at forward angles. Furthermore, since the leading order of the spectator expansion is not applicable at low energies, we only consider scattering at lab energies of 65 MeV or higher. As a result, the chiral expansion parameter becomes $Q = \max(p_{NA}, q)/\Lambda_b$. This expansion parameter is shown in Figure 2 for the case of $A = 4$ and $\Lambda_b = 600$ MeV. Because of the factorization of the c. m. momentum, there is a universal scattering angle at which the momentum transfer q begins to dominate the expansion parameter, regardless of the chosen E_{lab} or nucleus. We will exploit this behavior in later sections.

FIGURE 4
Differential cross section divided by Rutherford for proton scattering on ^{4}He at (first row) 65 MeV, (second row) 71 MeV, (third row) 100 MeV, and (fourth row) 200 MeV for LO (left column), NLO (middle column), and N2LO (right column) with corresponding 1σ (darker bands) and 2σ (lighter bands) error bands. Black dots are experimental data from Ref. [75] (65 MeV) [76], (71 MeV) [77], (100 MeV), and [78] (200 MeV).

4.1 Nuclear structure calculations

Prior to our detailed study of truncation uncertainties of a chiral NN interaction in elastic NA scattering observables we need to choose a specific chiral NN interaction. Here we want to focus on the EKM chiral NN interaction [18, 19] with a semi-local coordinate space regulator of R = 1 fm, which has a breakdown scale of Λ_b = 600 MeV. This interaction gives a slightly better description of the ground state energies in the upper p-shell than a similar, more recent interaction with a semi-local momentum space regulator. For consistency with the leading-order optical we only use the NN potentials, omitting three-nucleon forces, which appear at N2LO in the chiral expansion, both in the structure and the scattering part of the calculations. Including three-nucleon forces consistently in both, the structure and scattering calculations requires going beyond the leading-order optical potential, and is

beyond the scope of this work. Though initial attempts of incorporating three-nucleon forces as an effective density-dependent NN force in the scattering part have been presented [46], they can not yet be considered as systematic consideration of three-nucleon forces in NA scattering. For similar reasons, we restrict most of our results to N2LO since three-nucleon force contributions at N3LO and N4LO are significant [71].

Next, the translationally-invariant one-body density needed for the scattering calculation can be obtained using the NCSM approach, in which the nuclear wavefunction is expanded in Slater determinants of harmonic oscillator basis functions [30]. Ideally, one uses a sufficiently large basis to ensure convergence of this expansion, but in practice observables depend on both the many-body basis truncation, N_{max} (defined as the total number of harmonic oscillator quanta in the many-body system above the minimal

configuration), and on the harmonic oscillator scale $\hbar\Omega$. In Table 1 we give the ground state binding energies and point-proton radii of ^{4}He, ^{12}C, and ^{16}O obtained with the EKM chiral NN potential [18, 19] with a semi-local coordinate space regulator of R = 1 fm (note that at N2LO we did not include any three-nucleon forces).

For ^{4}He we can obtain nearly converged results for both the binding energy and the proton radius, and these results agree, to within their estimated numerical uncertainties (the first set of uncertainties in Table 1), with Yakubovsky calculations using the same NN potential [71]. However, for larger nuclei such as ^{12}C and ^{16}O we are more limited in the N_{max} values that can be reached on current computational resources.[1]

4.2 Pointwise truncation uncertainties

To assess the relative size of chiral truncation uncertainties compared to other known uncertainties, e.g. the harmonic oscillator parameters N_{max} and $\hbar\Omega$, we employ a pointwise truncation procedure and study reaction observables that are not functional quantities, e.g. reaction cross sections at a specified laboratory energy. This pointwise approach was previously implemented in Refs. [36, 43] and it starts by assuming the expansion parameter Q and reference scale y_{ref} are known. From there, we can apply Eq. 27 to calculate the coefficients c_n, which are treated as independent draws from the same underlying distribution. The properties of this distribution can be learned from Bayesian techniques and the posterior distribution for the prediction can be readily calculated with its associated credible intervals. For more details, see Ref. [36].

In order to estimate the chiral truncation uncertainties of the obtained ground state binding energies and radii, we apply the pointwise approach with $Q \approx .3$ as the effective expansion parameter, following Ref. [31]. These uncertainties are listed as the second set of uncertainties in Table 1, starting from NLO. Here we see that for the energies, the chiral uncertainties are at least of the same order as the estimated numerical uncertainties; however, the uncertainties of the radii of ^{12}C and ^{16}O are clearly dominated by their systematic dependence on the basis parameter $\hbar\Omega$.

---

[1] One commonly applies a Similarity Renormalization Group (SRG) transformation to the NN potential in order to improve the convergence of the many-body calculation. However, this leads to induced three-nucleon forces that are non-negligible; omitting those would lead to a strong dependence on the SRG parameter. We therefore choose to not employ such a transformation here. For the binding energies we use an exponential extrapolation to the complete basis, with associated uncertainties, see Ref. [71] for details. Radii converge rather slowly in a harmonic oscillator basis, and they do not necessarily converge monotonically with increasing N_{max}; furthermore, in the scattering calculations we use densities obtained at fixed values of the harmonic oscillator parameters N_{max} and $\hbar\Omega$. We therefore simply give in Table 1 our results for the point-proton radii of ^{12}C and ^{16}O at $N_{max} = 10$, averaged over the range $16 \le \hbar\Omega \le 28$ MeV (the same range as is used for the scattering calculations). The numerical uncertainty estimates for the radii listed in Table 1 correspond to the spread over this $\hbar\Omega$ interval; this is a systematic uncertainty due to the Gaussian fall-off of harmonic oscillator basis functions, and is therefore strongly correlated for the different chiral orders. However, the trend of a significant increase in the radii going from LO to NLO, followed by a smaller increase going from NLO to N2LO, is robust, and correlates with the decrease in binding energies going from LO to NLO to N2LO. Note that we did not include any chiral EFT corrections to the R^2 operator; and the experimental point-proton radii are extracted from the charge radius measured in electron scattering experiments, using standard proton and neutron finite-size corrections, relativistic corrections, and meson-exchange corrections.

To illustrate the pointwise approach for scattering observables, Figure 3 shows the reaction cross sections for proton scattering from ^{4}He at 65 MeV and ^{16}O at 100 MeV. For each case, the result is shown as a function of N_{max}, and variations with respect to $\hbar\Omega$ are indicated. While more obvious for the smaller nucleus where the NCSM can better converge, in both cases the uncertainty resulting from the chiral truncation remains larger than the uncertainty arising from the many-body method. To better illustrate this point, we present the reaction cross section for ^{4}He with a scale starting from 115 mb and with a range of only 45 mb, while using the full range of 600 mb for ^{16}O. While larger model spaces will better converge the NCSM results, smaller truncation uncertainties will only be achieved by higher chiral orders, despite the noticeable dependence of the radii on the harmonic oscillator parameter $\hbar\Omega$, in particular for the heavier nuclei, in the current calculations. Note however that even at N3LO we anticipate the chiral truncation uncertainties will be larger than the indicated variations with respect to the harmonic oscillator parameter $\hbar\Omega$ due to the rather large value of the expansion parameter Q in the scattering calculation.
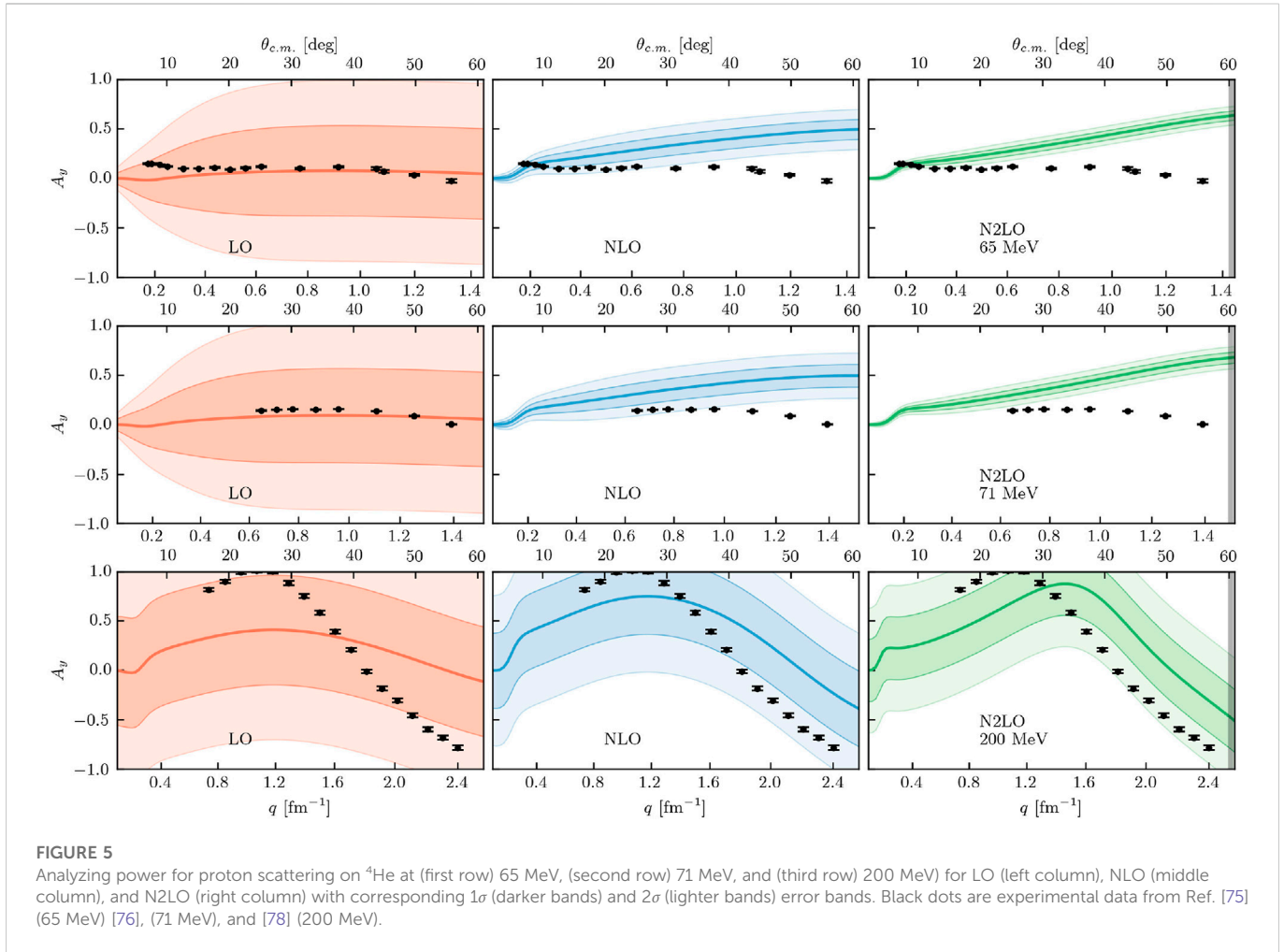
4.3 Correlated truncation uncertainties

For functional quantities $y(x)$ we employ a correlated approach that includes information at nearby values of x. This approach is better for observables such as a differential cross section, which we know does not vary wildly from values at nearby angles. It also starts from Eq. 27 and treats the coefficients $c_n(x)$ as independent draws from an underlying Gaussian process. This Gaussian process encodes information about the correlation length ℓ, and the qualities of the underlying distribution can be learned from the order-by-order results. This training is followed up by testing procedures which seek to confirm the Gaussian process has been appropriately fit to the available results, and if not, to diagnose potential issues. From a well-fit Gaussian process we can then extract truncation uncertainties for the functional quantities. For more details and applications, see Refs. [36, 43].

In the following examples, we examine proton scattering for ^{4}He, ^{12}C, and ^{16}O at various projectile energies and compare to the available experimental data. In each case, we show the convergence with respect to chiral order and the resulting decrease in the size of the chiral truncation uncertainties, as well as discuss any associated physics insights. To avoid concerns about the expansion parameter increasing at larger angles, we mostly restrict our analysis to forward angles where we expect the expansion parameter to be independent of the scattering angle.

For proton scattering on ^{4}He, we see good agreement with experiment for the differential cross sections (Figure 4) at lower projectile energies. Below 100 MeV, most data points fall within the 2σ uncertainty band, and at 100 MeV a majority of the data points are within the 1σ band. At the highest energy of 200 MeV, the chosen interaction seems unable to reproduce the experimental data, though this is not uncommon for scattering from ^{4}He.

The analyzing powers for proton scattering on ^{4}He (Figure 5) is more complicated. For the lower energies of 65 and 71 MeV, the experimental data shows a near zero value, regardless of scattering angle. In the scattering of a spin-1/2 particle from a spin-0 nucleus, this indicates that there is no spin-orbit force at play. This behavior is only reproduced by the LO result, for which the chiral NN interaction only contains the one-pion exchange and contact terms, which do not produce a spin-orbit force. At NLO the two-pion exchange diagrams are responsible for reproducing the NN p-waves and thus provide a spin-orbit force that

FIGURE 5
Analyzing power for proton scattering on ^{4}He at (first row) 65 MeV, (second row) 71 MeV, and (third row) 200 MeV) for LO (left column), NLO (middle column), and N2LO (right column) with corresponding 1σ (darker bands) and 2σ (lighter bands) error bands. Black dots are experimental data from Ref. [75] (65 MeV) [76], (71 MeV), and [78] (200 MeV).

leads to a non-zero value for the analyzing power in NA scattering. At N2LO there are no new terms in the two-nucleon sector, and thus A_y does not change its shape at that chiral order. Therefore, one needs to conclude that in this case other physics which goes beyond the leading order NA effective interaction may be needed to describe the analyzing power.
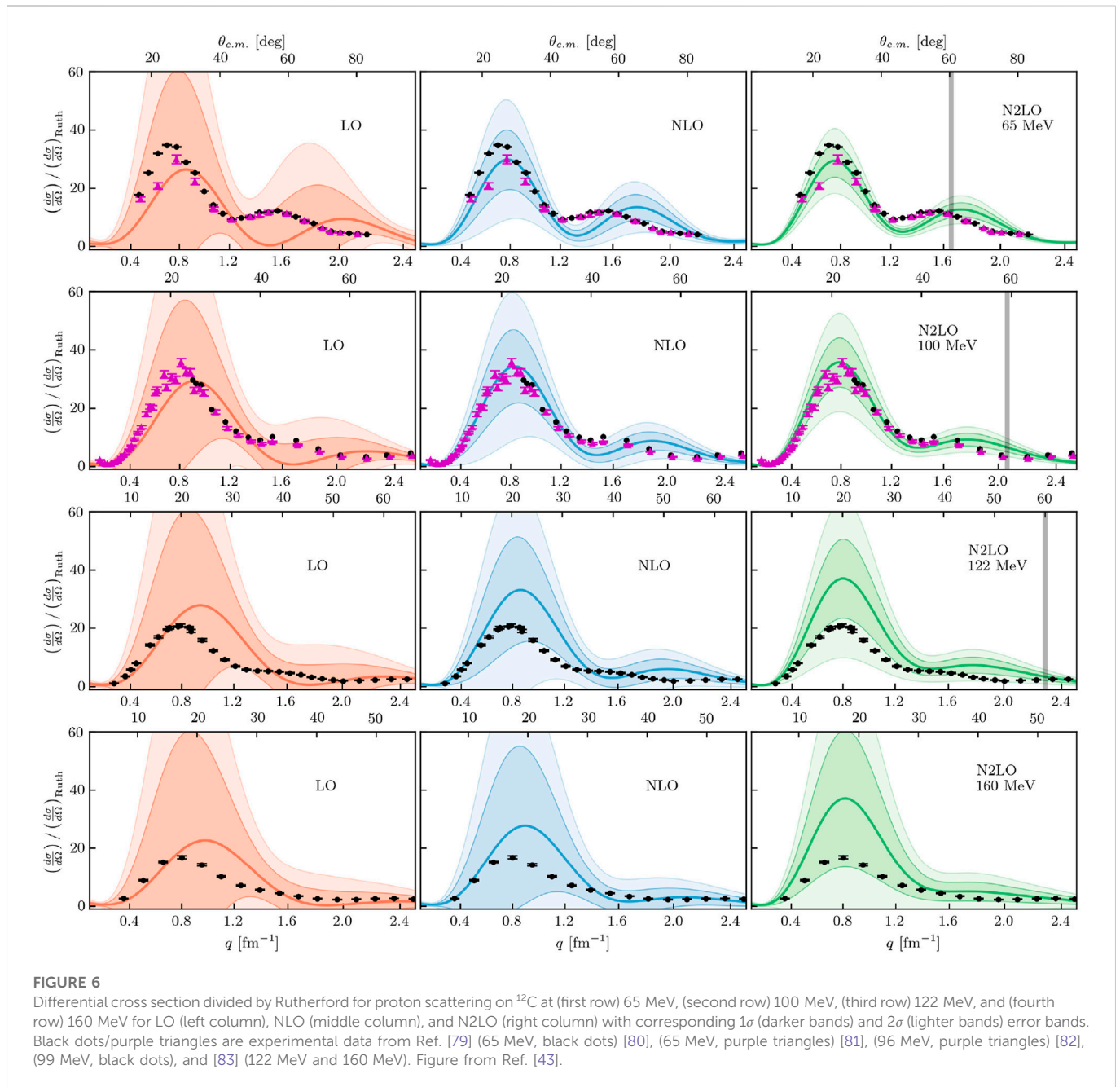
For the higher energy of 200 MeV, all of the experimental data points are within the 2σ uncertainty band, though there is a slight offset in the shape. In all cases, the analyzing power is more difficult to reproduce using this interaction, though other interactions have done better [39, 41].

For proton scattering from ^{12}C, the differential cross sections (Figure 6) are reliably reproduced by the central value of the N2LO calculations up to 100 MeV laboratory kinetic energy, and systematically over-predict at higher energies. As the projectile energy increases, the expansion parameter increases and as a result uncertainty bands become larger. This is most noticeable at 160 MeV: the experimental data is within the 1σ band, but the size of that band, as well as the 2σ band, are so large that they are not practically useful. The gray bars in the cross section panels for N2LO indicate the momentum transfer up to where we expect the expansion parameter to be dominated by the c. m. momentum p_{NA}. Once the momentum transfer exceeds the value given by the bar, the uncertainty is dominated by the momentum transfer q, and is thus underrepresented by the method we use. Note that the vertical bar is at the same scattering angle $\theta_{c.m.}$, but different momentum transfer q, as function of the projectile energy since p_{NA} is a function of the projectile energy as given in Eq. 29. Looking at the lower energies, the

increasing agreement with experiment in the first peak and minimum as higher orders in the chiral NN interaction are included gives the correct trend. Minima in the differential cross section correlate with the size of the target nucleus. It is well well known [31], and also evident from Table 1, that the nuclear binding energy calculated with the LO of the chiral NN interaction is way too large and correspondingly the radius much too small. Only when going to NLO and N2LO the binding energy as well as the radius move into the vicinity of their experimental values. This finding from structure calculations is corroborated by the calculations in Figure 6, where with increasing chiral order the calculated first diffraction minimum moves towards smaller momentum transfers indicating a larger nuclear size.

The analyzing powers for proton scattering on ^{12}C are at 65 MeV also almost zero for small momentum transfers and rise at $q = 1.2$ fm^{-1} to its maximum value of +1. This is captured by the NLO calculation where spin-contributions occur in the NN interaction (Figure 7). For 65 MeV, the experimental data is mostly within the 2σ band until approximately $\theta_{c.m.} = 60°$, where we expect the expansion parameter to being increasing and the uncertainty bands to thus be underestimates. For 122 MeV, the very forward direction is inside the 1σ band, but the overall shape of the experimental data is not well captured by this interaction.

For proton scattering from ^{16}O, the differential cross sections (Figure 8) are similar to the ^{12}C case. Namely, the lower energies do reasonably well at describing the data within the 2σ bands, but as the projectile energy increases the uncertainty bands increase to unhelpful

FIGURE 6
Differential cross section divided by Rutherford for proton scattering on ^{12}C at (first row) 65 MeV, (second row) 100 MeV, (third row) 122 MeV, and (fourth row) 160 MeV for LO (left column), NLO (middle column), and N2LO (right column) with corresponding 1σ (darker bands) and 2σ (lighter bands) error bands. Black dots/purple triangles are experimental data from Ref. [79] (65 MeV, black dots) [80], (65 MeV, purple triangles) [81], (96 MeV, purple triangles) [82], (99 MeV, black dots), and [83] (122 MeV and 160 MeV). Figure from Ref. [43].
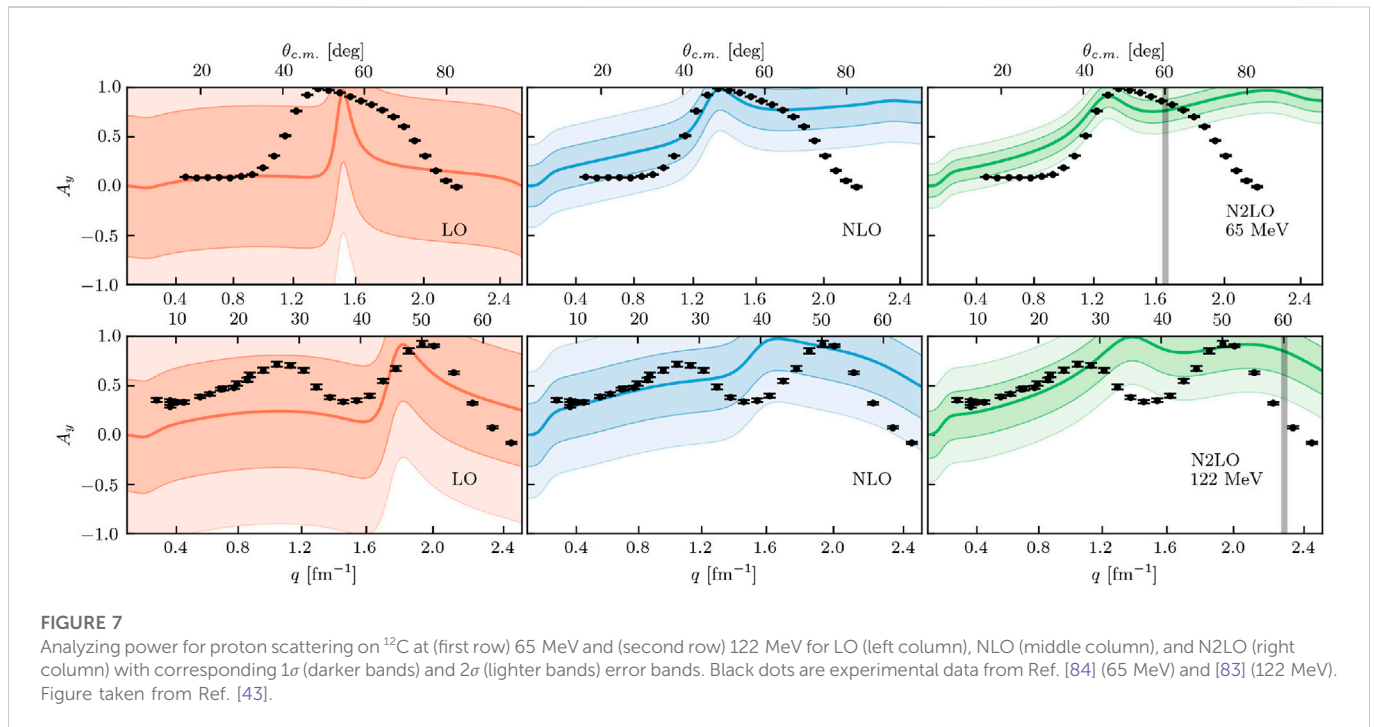
sizes. At the lowest energy of 65 MeV, we see a better and better reproduction of the first minimum in the differential cross section as the chiral order increases. Again, this first minimum is known to be related to the size of the nucleus, so this is an important feature to reproduce from both a structure, see Table 1, and reaction perspective.

The analyzing powers for proton scattering on ^{16}O (Figure 9) are again similar to the ^{12}C case. At lower energies (65 and 100 MeV), we again see a good reproduction to within 1σ or 2σ of the forward direction data, but beyond $\theta_{c.m.} = 60°$, the experimental data is outside the uncertainty bands. At the higher energy of 135 MeV, many of the experimental data are within the uncertainty bands but for a nucleus of this size, the expansion parameter has already increased such that the resulting uncertainty bands are unhelpfully large.

As stated toward the beginning of the section we omit three-nucleon forces for consistency with the leading-order optical potential which only

treats two active nucleons. Those three-nucleon forces already appear at N2LO in the chiral expansion, however, including them consistently in the structure as well as reaction calculation requires going beyond the leading-order optical potential and is beyond the scope of this work. For the sake of investigating truncation errors in the chiral NN force, one may carry out inconsistent calculation in the sense that the structure part of the calculation is kept fixed at N2LO, and in the reaction part higher orders in the NN force are used. Proceeding in this fashion is sensible, since the scattering calculation is more sensitive to the NN force compared to the structure calculation, provided this structure calculation gives a reasonable description of the ground state one-body density. To show how the chiral truncation error develops when higher chiral orders in the NN interaction are introduced, we show in Figure 10 proton scattering from ^{16}O at 100 MeV projectile energy, where the higher chiral orders are only employed in the scattering part through the corresponding Wolfenstein

FIGURE 7
Analyzing power for proton scattering on ^{12}C at (first row) 65 MeV and (second row) 122 MeV for LO (left column), NLO (middle column), and N2LO (right column) with corresponding 1σ (darker bands) and 2σ (lighter bands) error bands. Black dots are experimental data from Ref. [84] (65 MeV) and [83] (122 MeV). Figure taken from Ref. [43].

amplitudes. In both, the differential cross section as well as the analyzing power the two most right panels depicting the inconsistent calculation show that the uncertainty bands become smaller when higher chiral orders in the NN interaction are included. However, these uncertainty bands are not necessarily realistic due to missing higher-body effects, which include higher orders in the chiral force as well as higher orders in the multiple scattering expansion. Therefore, we can not draw firm conclusions from the fact that data are outside the uncertainty estimates. Nevertheless, it is obvious that the decrease in the uncertainties in the chiral truncation is rather slow due to the large expansion parameter. Furthermore, the medians of the calculations shown in Figures 8, 9 do not change when higher chiral orders are considered in Figure 10, which further indicates that the smaller error bands of the higher order chiral truncations may be artificial.
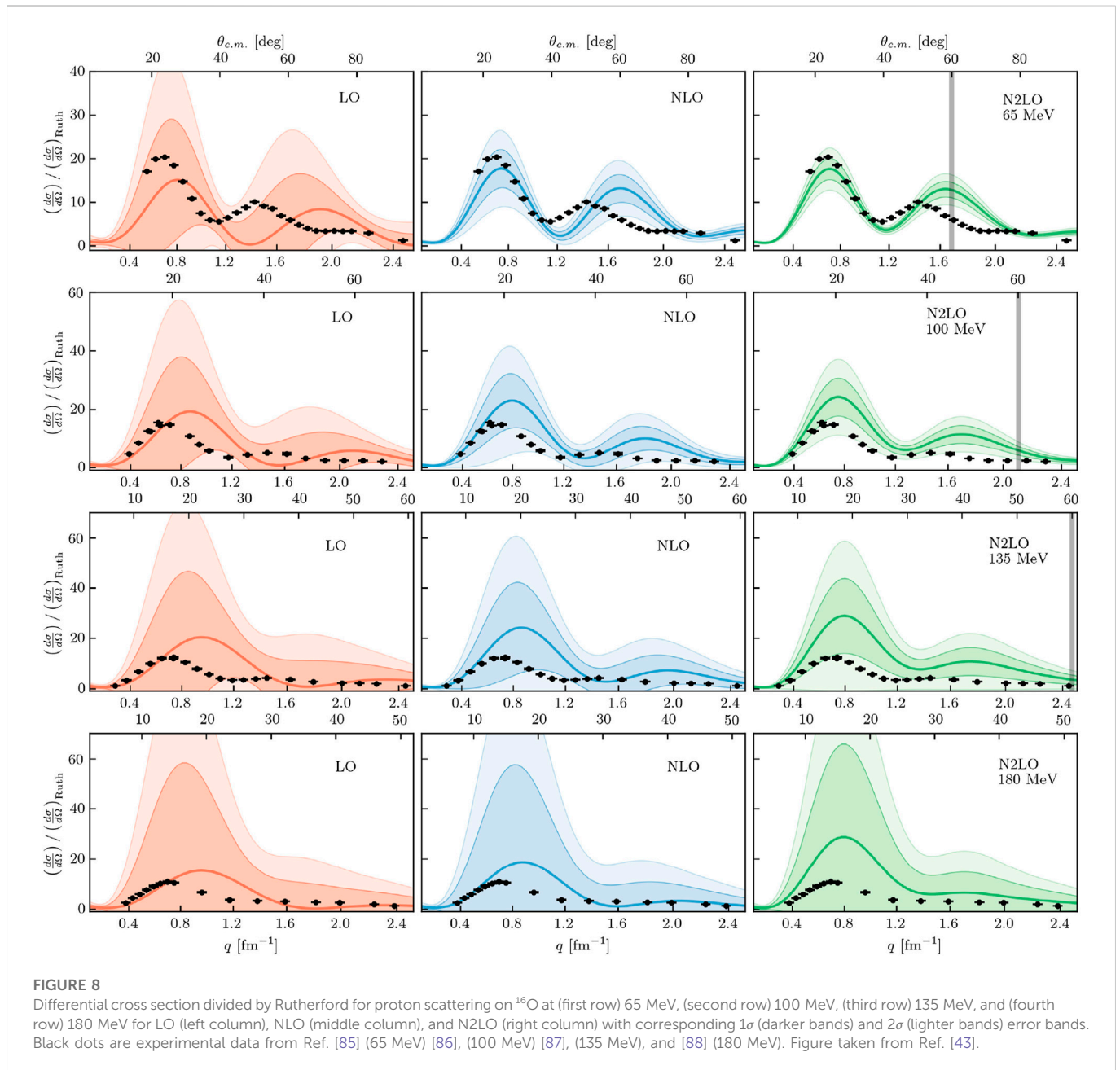
4.4 Analysis of posteriors

Even while restricting our analysis to a region where we expect the expansion parameter to be constant, we can still observe effects on the uncertainty bands if the expansion parameter is large, as noted in many of the results at larger projectile energies. In fact, this behavior will place limits on the size of nucleus that can be considered with this approach, since p_{NA} as defined by Eq. 29 will continue to increase as A increases, yielding $Q > 1$ eventually. While this situation is not ideal, we non-etheless find support for it in our analysis after examining the posteriors for Q, in accordance with Refs. [36, 43].

In Figure 11, we calculated posteriors for the differential cross sections in proton scattering from ^{4}He, ^{12}C, and ^{16}O at the energies previously discussed. From these, we can extract a single best guess for the value of Q based on the order-by-order calculations and compare that to the expectation for Q based on Eq. 30. For ^{16}O, the largest nucleus considered, we see generally good agreement between the expected value of Q and the best guess value from the posteriors (Figure 11C). However, as the nucleus decreases in size and as the laboratory energy

decreases, some differences begin to emerge between the two values. In Figure 11B for ^{12}C, the comparisons are roughly similar to the ^{16}O case, but for the ^{4}He analysis (Figure 11A), the differences are more pronounced, especially for the lower laboratory energies. A similar analysis of neutron scattering on ^{12}C did not show any significant differences between the two values [43], which implies ^{4}He may be the outlier in this approach. This analysis may imply scattering from ^{4}He with projectiles at lower energies could be analyzed with a smaller expansion parameter Q, though the higher energy results still favor the larger expansion parameter. As the smallest nucleus considered here, it may also point to the few-body character of ^{4}He, which has not historically been well captured in an optical potential approach.

5 Outlook

Procedures that quantify the theoretical uncertainties associated with the underlying chiral EFT NN interaction are by now well established for the NN and nucleon-deuteron systems as well as nuclear structure calculations, while the systematic study of chiral truncation uncertainty is not as widely used in *ab initio* effective interaction employed to describe the scattering of protons or neutrons from nuclei. Contributing factors for this relatively slow development include that when considering a multiple scattering approach to deriving this effective NA interaction in an *ab initio* fashion only recent progress in calculating the leading-order term in the multiple scattering approach has allowed to treat the NN interaction on the same footing in the structure and reaction part [41] by considering the spin of the struck target nucleon. Though calculations showed that the latter does not contribute significantly to observables when considering scattering from nuclei with a 0^+ ground state, one nevertheless needs a consistent *ab initio* implementation of the leading-order term of the effective NA interaction in order to study the

FIGURE 8
Differential cross section divided by Rutherford for proton scattering on ^{16}O at (first row) 65 MeV, (second row) 100 MeV, (third row) 135 MeV, and (fourth row) 180 MeV for LO (left column), NLO (middle column), and N2LO (right column) with corresponding 1σ (darker bands) and 2σ (lighter bands) error bands. Black dots are experimental data from Ref. [85] (65 MeV) [86], (100 MeV) [87], (135 MeV), and [88] (180 MeV). Figure taken from Ref. [43].
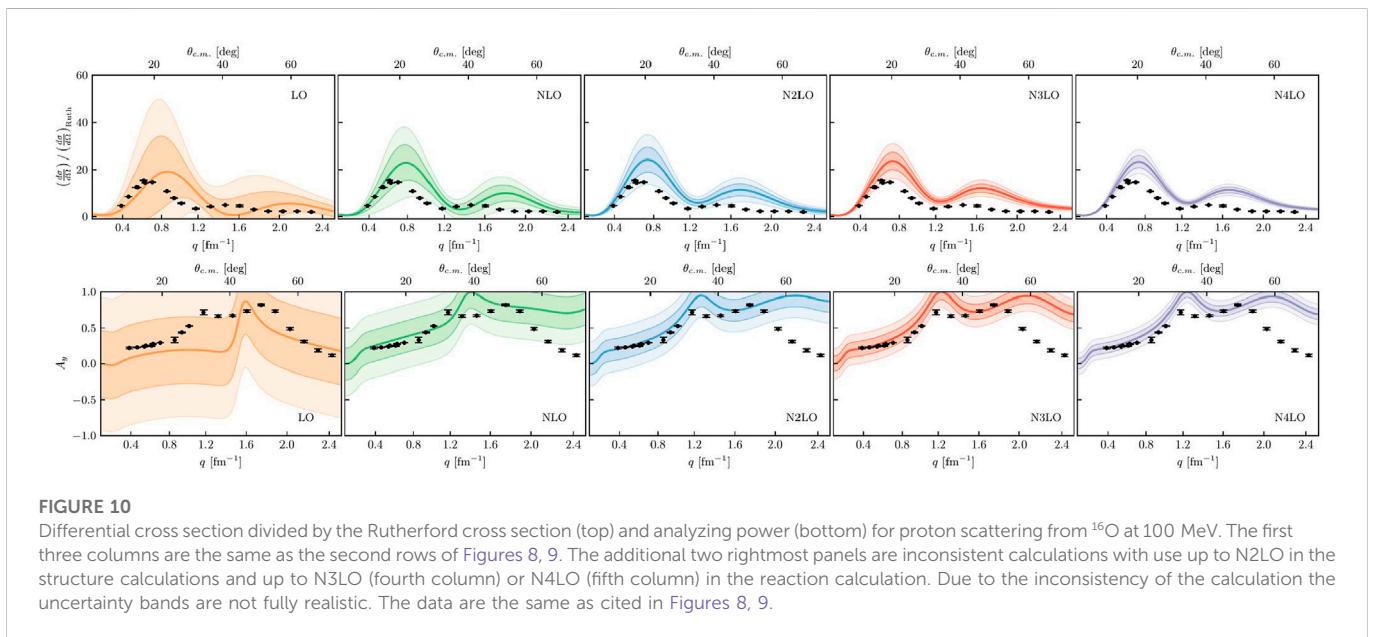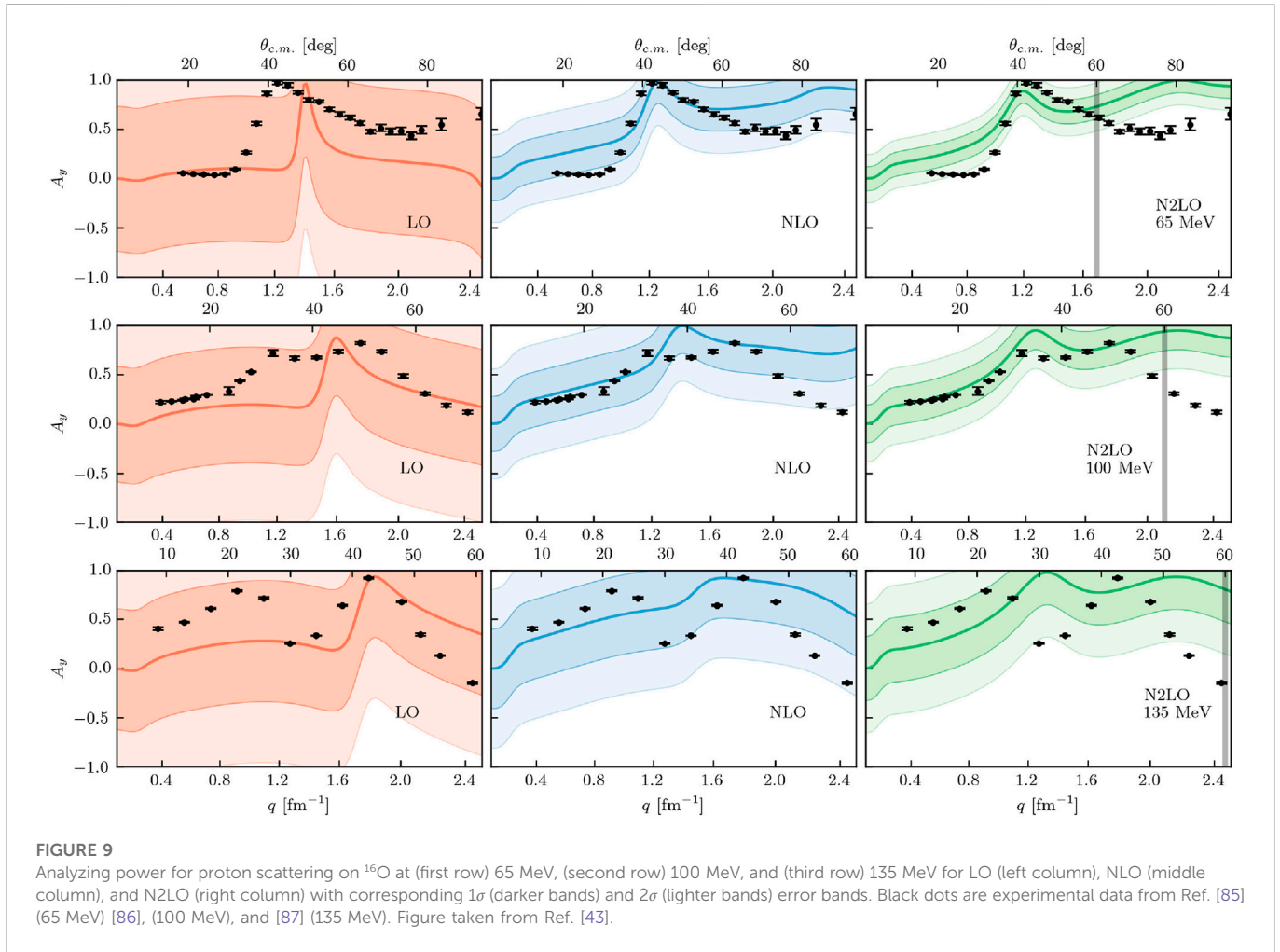
theoretical uncertainties imprinted on NA observables by the chiral EFT NN interaction.

In this work we carry out a systematic study of chiral truncation uncertainties of the EKM chiral interaction on the *ab initio* effective NA interaction calculated in leading order of the spectator expansion for ^4He, ^{12}C, and ^{16}O. We find that this interaction allows for a good description of experiment at energies around 100 MeV projectile kinetic energy and slightly lower, provided we focus on regions of momentum transfer where the analysis of the EFT truncation uncertainty is valid. When considering the lower energy of 65 MeV, the agreement with data starts to deteriorate. This is an indication that errors other than the truncation error in the chiral interaction should come into play, specifically errors that result from the spectator expansion itself. Theoretical consideration of the next-to-leading-order term in the spectator expansion are described in some detail in this work in order to lay out necessary theoretical and computational
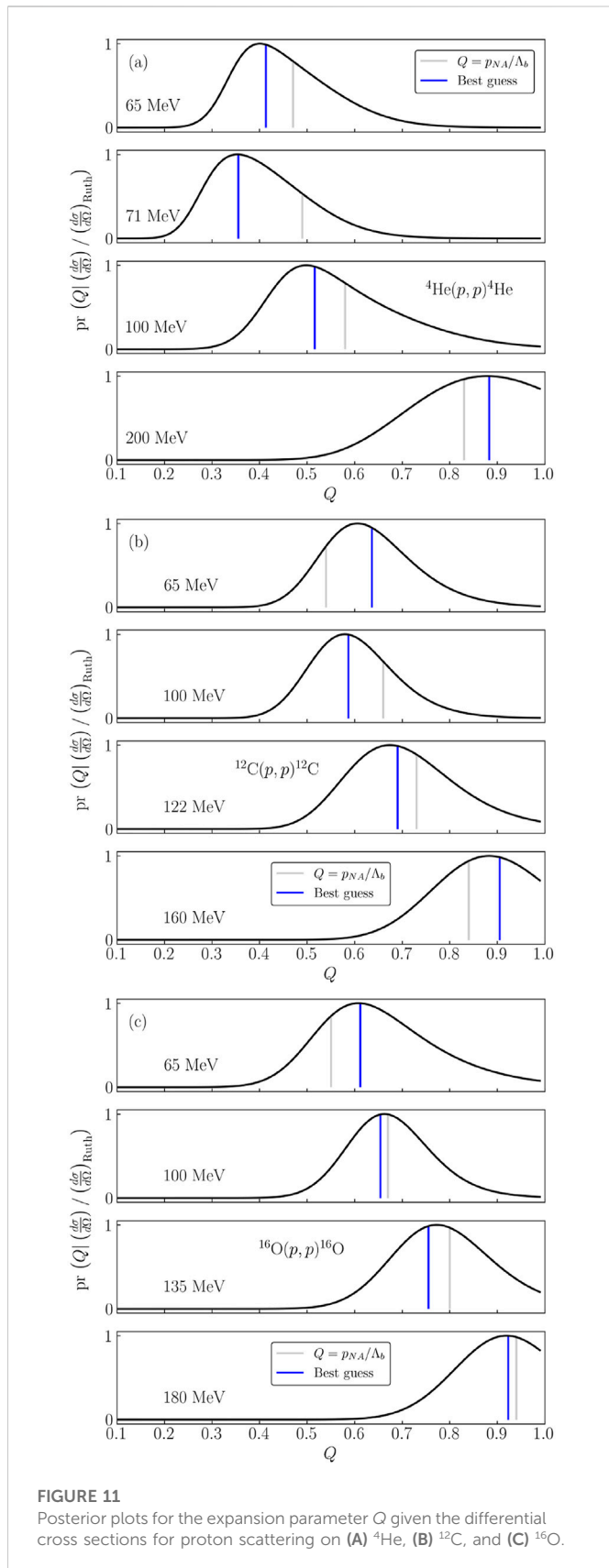
developments for this non-trivial endeavor. At at the next-to-leading order three-nucleon forces will naturally enter the effective interaction. At present this step has only been attempted in approximative fashions, namely by approximating the next-to-leading order in the propagator expansion *via* a nuclear mean field force [54] or by introducing an effective, density dependent NN potential in the scattering part of the calculation [46]. Since we are not considering next-to-leading order terms in the spectator expansion, we restrict our analysis to N2LO in the chiral interaction and only consider two-nucleon forces. In this case the choice of the EKM interaction with a semi-local coordinate space regulator of 1.0 fm is advantageous [38], since this specific interaction gives a slightly better description of the ground state energies in the upper *p*-shell compared to other more recent chiral EFT interactions when using two-nucleon interactions only.

In our study the chiral truncation errors at energies larger than 100 MeV increase considerably and the agreement with experiment

FIGURE 9
Analyzing power for proton scattering on ^{16}O at (first row) 65 MeV, (second row) 100 MeV, and (third row) 135 MeV for LO (left column), NLO (middle column), and N2LO (right column) with corresponding 1σ (darker bands) and 2σ (lighter bands) error bands. Black dots are experimental data from Ref. [85] (65 MeV) [86], (100 MeV), and [87] (135 MeV). Figure taken from Ref. [43].

FIGURE 10
Differential cross section divided by the Rutherford cross section (top) and analyzing power (bottom) for proton scattering from ^{16}O at 100 MeV. The first three columns are the same as the second rows of Figures 8, 9. The additional two rightmost panels are inconsistent calculations with use up to N2LO in the structure calculations and up to N3LO (fourth column) or N4LO (fifth column) in the reaction calculation. Due to the inconsistency of the calculation the uncertainty bands are not fully realistic. The data are the same as cited in Figures 8, 9.

deteriorates. The increase in the chiral truncation error can simply be traced back to the expansion parameter in our approach is getting too large. The deterioration of the agreement with experiment when going

to higher energies is more difficult to answer. One conclusion may be that the specific EKM chiral interaction employed here in using the leading-order in the spectator expansion is not well suited to describe

FIGURE 11
Posterior plots for the expansion parameter Q given the differential cross sections for proton scattering on **(A)** ^{4}He, **(B)** ^{12}C, and **(C)** ^{16}O.

features of a chiral NN interaction are most relevant for a description of NA scattering observables for light nuclei.

To put this in perspective, let us reconsider the basic ideas of the spectator expansion. By design, the leading-order term should be dominant at energies 150 MeV projectile kinetic energy and higher, since the reaction time of the projectile with nucleons inside the nucleus is short, and thus an 'impulse approximation' is in general very good. However, we do not want to consider here projectile energies larger than 400 MeV, where a relativistic treatment e.g. *via* the Dirac equation may be preferred [73, 74]. Thus at energies around 200 MeV the leading order term by design should give a reasonably good description of NA scattering data. This has been the case in the microscopic calculations of the 1990s (see e.g. [9–14]) and a set of recent calculations with specific chiral NN interactions [40, 41, 46]. Attempts to go beyond the leading order by incorporating 3NFs in a density dependent fashion into the many-body propagator [46] indicate that effects at 200 MeV are only visible at higher momentum transfer. In a similar fashion, investigations going beyond the leading order term in Ref. [54] indicate that those effects become important at around 100 MeV and at higher momentum transfers. Thus, if the 3NFs inherent in the chiral expansion are needed to influence calculations with chiral NN forces in the leading order of the spectator expansion at higher energies, then a new look at the interplay between NN and 3NFs in the leading-order spectator expansion must be developed.

Author contributions

All authors listed have made a substantial, direct, and intellectual contribution to the work and approved it for publication.

Funding

Acknowledgments

Conflict of interest

The authors declare that the research was conducted in the absence of any commercial or financial relationships that could be construed as a potential conflict of interest.

proton-nucleus scattering observables for ^{4}He, ^{12}C, and ^{16}O at higher energies. For the chiral NN interaction from Ref. [72] this is not the case as shown in Refs. [40, 41]. Therefore one will have to investigate what

Publisher's note

All claims expressed in this article are solely those of the authors and do not necessarily represent those of their affiliated organizations, or those of the publisher, the editors and the reviewers. Any product that may be evaluated in this article, or claim that may be made by its manufacturer, is not guaranteed or endorsed by the publisher.

References

1. Bethe HA. Theory of disintegration of nuclei by neutrons. *Phys Rev* (1935) 47:747–59. doi:10.1103/PhysRev.47.747

2. Feshbach H. The optical model and its justification. *Annu Rev Nucl Sci* (1958) 8: 49–104. doi:10.1146/annurev.ns.08.120158.000405

3. Watson KM. Multiple scattering and the many-body problem-applications to photomeson production in complex nuclei. *Phys Rev* (1953) 89:575–87. doi:10.1103/physrev.89.575

4. Francis NC, Watson KM. The elastic scattering of particles by atomic nuclei. *Phys Rev* (1953) 92:291–303. doi:10.1103/physrev.92.291

5. Kerman AK, McManus H, Thaler RM. The scattering of fast nucleons from nuclei. *Ann Phys* (1959) 8:551–635. doi:10.1016/0003-4916(59)90076-4

6. Siciliano ER, Thaler RM. Spectator expansion in multiple scattering theory. *Phys Rev C* (1977) 16:1322–32. doi:10.1103/PhysRevC.16.1322

7. Ernst DJ, Londergan JT, Miller GA, Thaler RM. Correlation expansion of the optical potential. *Phys Rev C* (1977) 16:537–55. doi:10.1103/PhysRevC.16.537

8. Tandy PC, Thaler RM. Multiple scattering expansion with distortion. *Phys Rev C* (1980) 22:2321–9. doi:10.1103/PhysRevC.22.2321

9. Crespo R, Johnson RC, Tostevin JA. Multiple scattering theory of proton elastic scattering at intermediate energies. *Phys Rev C* (1992) 46:279–97. doi:10.1103/PhysRevC. 46.279

10. Crespo R, Johnson RC, Tostevin JA. Full folding calculations for proton-nucleus elastic scattering at intermediate energies. *Phys Rev C* (1990) 41:2257–62. doi:10.1103/PhysRevC.41.2257

11. Elster C, Weppner SP, Chinn CR. Full-folding optical potentials for elastic nucleon-nucleus scattering based on realistic densities. *Phys Rev C* (1997) 56:2080–92. doi:10.1103/PhysRevC.56.2080

12. Elster C, Cheon T, Redish EF, Tandy PC. Full-folding optical potentials in elastic proton-nucleus scattering. *Phys Rev C* (1990) 41:814–27. doi:10.1103/PhysRevC.41.814

13. Arellano HF, Brieva FA, Love WG. Nonrelativistic full-folding model of nucleon elastic scattering at intermediate energies. *Phys Rev C* (1990) 41:2188–201. 10.1103/PhysRevC.42.1782. [Erratum: Phys. Rev.C 42, 1782 (1990)]. doi:10.1103/PhysRevC.41.2188

14. Arellano HF, Brieva FA, Love WG. Role of nuclear densities in nucleon elastic scattering. *Phys Rev C* (1990) 42:652–8. doi:10.1103/PhysRevC.42.652

15. Entem DR, Machleidt R. *Phys Rev C* (2003) 68:041001. doi:10.1103/physrevc.68.041001

16. Epelbaum E. Few-nucleon forces and systems in chiral effective field theory. *Prog Part Nucl Phys* (2006) 57:654–741. doi:10.1016/j.ppnp.2005.09.002

17. Epelbaum E, Hammer HW, Meißner UG. Modern theory of nuclear forces. *Rev Mod Phys* (2009) 81:1773–825. doi:10.1103/RevModPhys.81.1773

18. Epelbaum E, Krebs H, Meißner UG. Precision nucleon-nucleon potential at fifth order in the chiral expansion. *Phys Rev Lett* (2015) 115:122301. doi:10.1103/PhysRevLett.115.122301

19. Epelbaum E, Krebs H, Meißner UG. Improved chiral nucleon-nucleon potential up to next-to-next-to-next-to-leading order. *Eur Phys J A* (2015) 51:53. doi:10.1140/epja/i2015-15053-8

20. Reinert P, Krebs H, Epelbaum E. Semilocal momentum-space regularized chiral two-nucleon potentials up to fifth order. *Eur Phys J A* (2018) 54:86. doi:10.1140/epja/i2018-12516-4

21. Machleidt R, Entem DR. Chiral effective field theory and nuclear forces. *Phys Rep* (2011) 503:1–75. doi:10.1016/j.physrep.2011.02.001

22. Entem DR, Machleidt R, Nosyk Y. High-quality two-nucleon potentials up to fifth order of the chiral expansion. *Phys Rev C* (2017) 96:024004. doi:10.1103/PhysRevC.96.024004

23. Langr D, Dytrych T, Draayer JP, Launey KD, Tvrdík P. Efficient algorithm for representations of U(3) in U(N). *Comput Phys Commun* (2019) 244:442–7. doi:10.1016/j.cpc.2019.05.018

24. Langr D, Dytrych T, Launey KD, Draayer JP. Accelerating many-nucleon basis generation for high performance computing enabled *ab initio* nuclear structure studies. *Int J High Perform Comput Appl* (2019) 33:522–33. doi:10.1177/1094342019838314

25. Shao M, Aktulga HM, Yang C, Ng EG, Maris P, Vary JP. Accelerating nuclear configuration interaction calculations through a preconditioned block iterative eigensolver. *Comput Phys Commun* (2018) 222:1–13. doi:10.1016/j.cpc.2017.09.004

26. Aktulga HM, Yang C, Ng EG, Maris P, Vary JP. Improving the scalability of a symmetric iterative eigensolver for multi-core platforms. *Concurrency Computat.: Pract Exper* (2014) 26:2631–51. doi:10.1002/cpe.3129

27. Jung M, Wilson EH, III, Choi W, Shalf J, Aktulga HM, Yang C, et al. Exploring the future of out-of-core computing with compute-local non-volatile memory. In: SC '13: Proceedings of the International Conference on High Performance Computing, Networking, Storage and Analysis. New York, NY, USA: ACM (2013). p. 75:1–75:11. doi:10.1145/2503210.2503261

28. Navrátil P, Vary JP, Barrett BR. Properties of12Cin theAb InitioNuclear shell model. *Phys Rev Lett* (2000) 84:5728–31. doi:10.1103/PhysRevLett.84.5728

29. Roth R, Navrátil P. Ab InitioStudy ofCa40with an importance-truncated No-core shell model. *Phys Rev Lett* (2007) 99:092501. doi:10.1103/PhysRevLett.99.092501

30. Barrett B, Navrátil P, Vary J. *Ab initio* no core shell model. *Prog Part Nucl Phys* (2013) 69:131–81. doi:10.1016/j.ppnp.2012.10.003

31. Binder S, Calci A, Epelbaum E, Furnstahl RJ, Golak J, Hebeler K, et al. Few-nucleon and many-nucleon systems with semilocal coordinate-space regularized chiral nucleon-nucleon forces. *Phys Rev C* (2018) 98:014002. doi:10.1103/PhysRevC.98.014002

32. Launey KD, Dytrych T, Draayer JP. Symmetry-guided large-scale shell-model theory. *Prog Part Nucl Phys* (2016) 89:101–36. doi:10.1016/j.ppnp.2016.02.001

33. Dytrych T, Launey KD, Draayer JP, Rowe DJ, Wood JL, Rosensteel G, et al. Physics of nuclei: Key role of an emergent symmetry. *Phys Rev Lett* (2020) 124:042501. doi:10.1103/PhysRevLett.124.042501

34. Furnstahl RJ, Klco N, Phillips DR, Wesolowski S. Quantifying truncation errors in effective field theory. *Phys Rev C* (2015) 92:024005. doi:10.1103/PhysRevC.92.024005

35. Melendez JA, Wesolowski S, Furnstahl RJ. Bayesian truncation errors in chiral effective field theory: Nucleon-nucleon observables. *Phys Rev C* (2017) 96:024003. doi:10.1103/PhysRevC.96.024003

36. Melendez JA, Furnstahl RJ, Phillips DR, Pratola MT, Wesolowski S. Quantifying correlated truncation errors in effective field theory. *Phys Rev C* (2019) 100:044001. doi:10.1103/PhysRevC.100.044001

37. Epelbaum E, Golak J, Hebeler K, Kamada H, Krebs H, Meißner G, et al. Towards high-order calculations of three-nucleon scattering in chiral effective field theory. *Eur Phys J A* (2020) 56:92. doi:10.1140/epja/s10050-020-00102-2

38. Maris P, Epelbaum E, Furnstahl RJ, Golak J, Hebeler K, Hüther T, et al. Light nuclei with semilocal momentum-space regularized chiral interactions up to third order. *Phys Rev C* (2021) 103:054001. doi:10.1103/PhysRevC.103.054001

39. Burrows M, Elster C, Popa G, Launey KD, Nogga A, Maris P. *Ab initio* translationally invariant nonlocal one-body densities from No-core shell-model theory. *Phys Rev C* (2018) 97:024325. doi:10.1103/PhysRevC.97.024325

40. Burrows M, Elster C, Weppner SP, Launey KD, Maris P, Nogga A, et al. *Ab initio* folding potentials for nucleon-nucleus scattering based on NCSM one-body densities. *Phys Rev C* (2019) 99:044603. doi:10.1103/physrevc.99.044603

41. Burrows M, Baker RB, Elster C, Weppner SP, Launey KD, Maris P, et al. *Ab initio* leading order effective potentials for elastic nucleon-nucleus scattering. *Phys Rev C* (2020) 102:034606. doi:10.1103/PhysRevC.102.034606

42. Baker RB, Burrows M, Elster C, Launey KD, Maris P, Popa G, et al. Nuclear spin features relevant to *ab initio* nucleon-nucleus elastic scattering. *Phys Rev C* (2021) 103: 054314. doi:10.1103/PhysRevC.103.054314

43. Baker RB, McClung B, Elster C, Maris P, Weppner SP, Burrows M, et al. *Ab initio* nucleon-nucleus elastic scattering with chiral effective field theory uncertainties. *Phys Rev C* (2022) 106:064605. doi:10.1103/PhysRevC.106.064605

44. Gennari M, Vorbbi M, Calci A, Navrátil P. Microscopic optical potentials derived from *ab initio* translationally invariant nonlocal one-body densities. *Phys Rev C* (2018) 97: 034619. doi:10.1103/PhysRevC.97.034619

45. Vorabbi M, Gennari M, Finelli P, Giusti C, Navrátil P, Machleidt R. Elastic proton scattering off nonzero spin nuclei. *Phys Rev C* (2022) 105:014621. doi:10.1103/PhysRevC.105.014621

46. Vorabbi M, Gennari M, Finelli P, Giusti C, Navrátil P, Machleidt R. Impact of three-body forces on elastic nucleon-nucleus scattering observables. *Phys Rev C* (2021) 103: 024604. doi:10.1103/PhysRevC.103.024604

47. Arellano HF, Blanchon G. On the separability of microscopic optical model potentials and emerging bell-shape Perey-Buck nonlocality. *Eur Phys J A* (2022) 58: 119. doi:10.1140/epja/s10050-022-00777-9

48. Feshbach H. Unified theory of nuclear reactions. *Ann Phys* (1958) 5:357–90. doi:10.1016/0003-4916(58)90007-1

49. Dickhoff WH, Barbieri C. Self-consistent Green's function method for nuclei and nuclear matter. *Prog Part Nucl Phys* (2004) 52:377–496. doi:10.1016/j.ppnp.2004.02.038

50. Idini A, Barbieri C, Navrátil P. *Ab initio* optical potentials and nucleon scattering on medium mass nuclei. *Phys Rev Lett* (2019) 123:092501. doi:10.1103/PhysRevLett.123.092501

51. Rotureau J, Danielewicz P, Hagen G, Nunes FM, Papenbrock T. Optical potential from first principles. *Phys Rev C* (2017) 95:024315. doi:10.1103/PhysRevC.95.024315

52. Launey KD, Mercenne A, Dytrych T. Nuclear dynamics and reactions in the ab initio symmetry-adapted framework. *Annu Rev Nucl Part Sci* (2021) 71:253–77. doi:10.1146/annurev-nucl-102419-033316

53. Hebborn C, Nunes FM, Potel G, Dickhoff WH, Holt JW, Atkinson MC, et al. *Optical potentials for the rare-isotope beam era* (2022). arXiv:2210.07293.

54. Chinn CR, Elster C, Thaler RM, Weppner SP. Propagator modifications in elastic nucleon-nucleus scattering within the spectator expansion. *Phys Rev C* (1995) 52:1992–2003. doi:10.1103/PhysRevC.52.1992

55. Chinn CR, Elster C, Thaler RM. Isospin effects in elastic proton-nucleus scattering. *Phys Rev C* (1993) 47:2242–9. doi:10.1103/PhysRevC.47.2242

56. Miller GA, Austern N, Silver M. Vanishing closure correction in the second-order optical potential. *Phys Rev C* (1978) 17:835–6. doi:10.1103/PhysRevC.17.835

57. Chinn CR, Elster C, Thaler RM. Microscopic formulation of medium contributions to the first-order optical potential. *Phys Rev C* (1993) 48:2956–66. doi:10.1103/PhysRevC.48.2956

58. Chinn CR, Elster C, Thaler RM, Weppner SP. Application of multiple scattering theory to lower-energy elastic nucleon-nucleus scattering. *Phys Rev C* (1995) 51:1418–24. doi:10.1103/PhysRevC.51.1418

59. Wolfenstein L, Ashkin J. Invariance conditions on the scattering amplitudes for spin ½ particles. *Phys Rev* (1952) 85:947–9. doi:10.1103/physrev.85.947

60. Fachruddin I, Elster C, Glöckle W. Nucleon-nucleon scattering in a three dimensional approach. *Phys Rev C* (2000) 62:044002. doi:10.1103/PhysRevC.62.044002

61. Golak J, Glöckle W, Skibiński R, Witała H, Rozpędzik D, Topolnicki K, et al. Two-nucleon systems in three dimensions. *Phys Rev C* (2010) 81:034006. doi:10.1103/PhysRevC.81.034006

62. Burrows M. *Ab initio leading order effective interactions for scattering of nucleons from light nuclei*. Ph.D. thesis. Athens, Ohio: Ohio University (2020).

63. Cunningham ES, Al-Khalili JS, Johnson RC. Role of the tensor exchange potential in nucleon-nucleus scattering. *Phys Rev C* (2011) 84:041601. doi:10.1103/PhysRevC.84.041601

64. Cunningham ES, Al-Khalili JS, Johnson RC. Effect of spin-spin interactions on nucleon-nucleus scattering. *Phys Rev C* (2013) 87:054601. doi:10.1103/PhysRevC.87.054601

65. Møller C. *K Dan Vidensk Sels Mat Fys Medd* (1945) 23:1.

66. Rodberg L, Thaler R. Introduction of the quantum theory of scattering. In: *Pure and applied physics*, Vol. 26. Cambridge, MA, USA: Academic Press (1967).

67. Navrátil P. Translationally invariant density. *Phys Rev C* (2004) 70:014317. doi:10.1103/PhysRevC.70.014317

68. Cockrell C, Vary JP, Maris P. Lithium isotopes within the ab initio no-core full configuration approach. *Phys Rev C* (2012) 86:034325. doi:10.1103/PhysRevC.86.034325

69. Mihaila B, Heisenberg JH. Center-of-mass corrections reexamined: A many-body expansion approach. *Phys Rev C* (1999) 60:054303. doi:10.1103/PhysRevC.60.054303

70. Navrátil P. Translationally invariant matrix elements of general one-body operators. *Phys Rev C* (2021) 104:064322. doi:10.1103/PhysRevC.104.064322

71. Binder S, Calci A, Epelbaum E, Furnstahl RJ, Golak J, Hebeler K, et al. Few-nucleon systems with state-of-the-art chiral nucleon-nucleon forces. *Phys Rev C* (2016) 93:044002. doi:10.1103/PhysRevC.93.044002

72. Ekström A, Baardsen G, Forssén C, Hagen G, Hjorth-Jensen M, Jansen GR, et al. Optimized chiral nucleon-nucleon interaction at next-to-next-to-leading order. *Phys Rev Lett* (2013) 110:192502. doi:10.1103/physrevlett.110.192502

73. Cooper ED, Hama S, Clark BC, Mercer RL. Global Dirac phenomenology for proton-nucleus elastic scattering. *Phys Rev C* (1993) 47:297–311. doi:10.1103/PhysRevC.47.297

74. Hynes MV, Picklesimer A, Tandy PC, Thaler RM. Relativistic (Dirac equation) effects in microscopic elastic scattering calculations. *Phys Rev C* (1985) 31:1438–63. doi:10.1103/PhysRevC.31.1438

75. Imai K, Hatanaka K, Shimizu H, Tamura N, Egawa K, Nisimura K, et al. Polarization and cross section measurements for p-4he elastic scattering at 45, 52, 60 and 65 mev. *Nucl Phys A* (1979) 325:397–407. doi:10.1016/0375-9474(79)90023-X

76. Burzynski S, Campbell J, Hammans M, Henneck R, Lorenzon WB, Pickar MA, et al. p–4He scattering: New data and a phase-shift analysis between 30 and 72 MeV. *Phys Rev C* (1989) 39:56–64. doi:10.1103/PhysRevC.39.56

77. Goldstein NP, Held A, Stairs DG. Elastic scattering of 100 mev protons from 3he and 4he. *Can J Phys* (1970) 48:2629–39. doi:10.1139/p70-326

78. Moss GA, Greeniaus LG, Cameron JM, Hutcheon DA, Liljestrand RL, Miller CA, et al. Proton-He4 elastic scattering at intermediate energies. *Phys Rev C* (1980) 21:1932–43. doi:10.1103/PhysRevC.21.1932

79. Ieiri M, Sakaguchi H, Nakamura M, Sakamoto H, Ogawa H, Yosol M, et al. A multifoil carbon polarimeter for protons between 20 and 84 mev. *Nucl Instr Methods Phys Res Section A: Acc Spectrometers, Detectors Associated Equipment* (1987) 257:253–78. doi:10.1016/0168-9002(87)90744-3

80. Kato S, Okada K, Kondo M, Hosono K, Saito T, Matsuoka N, et al. Inelastic scattering of 65 mev protons from ^{12}C, ^{24}Mg, ^{28}Si, and ^{32}S. *Phys Rev C* (1985) 31:1616–32. doi:10.1103/PhysRevC.31.1616

81. Strauch K, Titus F. Direct excitation of nuclear energy states in carbon by 96-mev protons. *Phys Rev* (1956) 103:200–8. doi:10.1103/PhysRev.103.200

82. Gerstein G, Niederer J, Strauch K. Elastic scattering of 96-mev protons. *Phys Rev* (1957) 108:427–32. doi:10.1103/PhysRev.108.427

83. Meyer HO, Schwandt P, Jacobs WW, Hall JR. Proton scattering from C12 between 120 and 200 MeV and the optical potential. *Phys Rev C* (1983) 27:459–69. doi:10.1103/PhysRevC.27.459

84. Ieiri M, Sakaguchi H, Nakamura M, Sakamoto H, Ogawa H, Yosol M, et al. A multifoil carbon polarimeter for protons between 20 and 84 mev. *Nucl Instr Methods Phys Res Section A: Acc Spectrometers, Detectors Associated Equipment* (1987) 257:253–78. doi:10.1016/0168-9002(87)90744-3

85. Sakaguchi H, Nakamura M, Hatanaka K, Goto A, Noro T, Ohtani F, et al. 65 MeV polarized proton elastic scattering and the effective two-body interaction range. *Phys Lett B* (1979) 89:40–3. doi:10.1016/0370-2693(79)90071-6

86. Seifert H. *Energy dependence of the effective interaction for nucleon-nucleus scattering*. Ph.D. thesis. College Park, Maryland: University of Maryland (1990).

87. Kelly JJ, Bertozzi W, Buti TN, Finn JM, Hersman FW, Hyde-Wright C, et al. Density dependence in the two-nucleon effective interaction at 135 MeV. *Phys Rev C* (1989) 39:1222–41. doi:10.1103/PhysRevC.39.1222

88. Kelly JJ, Finn JM, Bertozzi W, Buti TN, Hersman FW, Hyde-Wright C, et al. Effective interactions and nuclear structure using 180 MeV protons. I.O16(p,p'). *Phys Rev C* (1990) 41:2504–13. doi:10.1103/PhysRevC.41.2504